Journal of Elasticity **30**: 123–189, 1993.

Coupled shear-torsional motion of a rubber support system

ZILIANG ZHOU
Department of Mechanical Engineering and Applied Mechanics, The University of Michigan, Ann Arbor, MI 48109, USA

Received 4 December 1990; in revised form 20 April 1992

Abstract. The finite amplitude, coupled shear-torsional motion of a circular disk supported between identical rubber spring cylinders is studied. The material of the springs is assumed to be an incompressible elastic material. The oscillatory motion of the disk is studied for two different cases. In the first case, the material of the spring is assumed to be an incompressible elastic material whose response functions are constants. Typical examples include the Mooney-Rivlin model. The motion of the disk in this case is governed by two independent equations whose closed form solutions are noted. For the second case, the material of the spring is assumed to be an incompressible quadratic material. The motion of the disk in this case is governed by two coupled nonlinear differential equations. The stability properties of small shearing oscillation superimposed on finite torsion and small torsional oscillation superimposed on finite shearing are studied.

AMS (MOS) subject classification: 73D35 or 73C50.

1. Introduction

Simple shear and pure torsion have been studied separately in numerous cases. Important results have been noted, such as the universal relations [1], static and dynamic responses of oscillating systems [2], and stability of the motions involved in various engineering applications [3, 4]. The coupled shear-torsional motion which is observed in a variety of engineering design applications, however, has not received enough attention. The purpose of this work is to give a comprehensive description of the motion. Physically, we are going to consider the motion of a circular disk supported between identical rubber cylinders. After a brief review of the basic principles of continuum mechanics in §2, the kinematics of the motion is studied in §3. The Cauchy stress tensor is then determined for a class of incompressible elastic materials in §4. The equations of motion of the disk supported by the coupled rubber springs are derived in §5. The closed form solutions are provided in §6 for a class of incompressible elastic materials whose response functions are constants. Then, the equations of motion of the disk are obtained for an incompressible quadratic spring support in §7. We then turn to the oscillation problem involving concurrent finite torsion and small shearing motion of the

disk. The exact solution to the finite amplitude torsional motion is derived in terms of the elliptic integral of the first kind. The small, coupled shearing motion is reduced to Hill's equation whose stability properties are discussed in §8. Finally, we look at finite shearing coupled with small torsion. The mathematical structure of this problem is the same as the one studied in §8. The exact solution for finite shearing and the stability of small torsion are discussed in §9.

2. Basic equations of continuum mechanics

We consider a body in a Euclidean space of three dimensions to undergo a deformation described by

$$\mathbf{x} = \mathbf{x}(\mathbf{X}, t), \tag{2.1}$$

where $\mathbf{x}$ and $\mathbf{X}$ are the respective position vectors of a typical particle of the body at an arbitrary time t and a reference time t_R. The velocity $\mathbf{v}$ and the acceleration $\mathbf{a}$ of the particle are defined by

$$\mathbf{v}(\mathbf{X}, t) \equiv \dot{\mathbf{x}}(\mathbf{X}, t), \quad \mathbf{a}(\mathbf{X}, t) \equiv \dot{\mathbf{v}}(\mathbf{X}, t) = \ddot{\mathbf{x}}(\mathbf{X}, t), \tag{2.2}$$

where the superimposed dot denotes the usual material time derivative.

We recall the deformation gradient $\mathbf{F}$ and the Cauchy-Green deformation tensor $\mathbf{B}$ defined by

$$\mathbf{F} \equiv \frac{\partial \mathbf{x}(\mathbf{X}, t)}{\partial \mathbf{X}}, \quad \mathbf{B} \equiv \mathbf{F}\mathbf{F}^T. \tag{2.3}$$

An isotropic and incompressible, hyperelastic solid is a material whose constitutive equation is given by

$$\mathbf{T} = -p\mathbf{1} + \beta_1 \mathbf{B} + \beta_{-1}\mathbf{B}^{-1}, \tag{2.4}$$

where $\mathbf{T}$ is the Cauchy stress tensor and p is the undetermined pressure due to the incompressibility constraint. The response functions β_1 and β_{-1} are functions of the principal invariants of $\mathbf{B}$ and can be derived from the strain energy function. A typical example is the Mooney-Rivlin material whose response functions are given by [5]

$$\beta_1 = \frac{G}{1+\alpha}, \quad \beta_{-1} = -\frac{\alpha G}{1+\alpha}, \tag{2.5}$$

where G is the shear modulus and α is a positive material parameter, usually between 0 and 1. When $\alpha = 0$, the Mooney-Rivlin model reduces to the well-known neo-Hookean model. Another model that will be used in this work is the quadratic material defined as [6]

$$\Sigma = C_1(I_1 - 3) + C_2(I_2 - 3) + C_3(I_1 - 3)^2 + C_4(I_2 - 3)^2$$

$$+ C_5(I_1 - 3)(I_2 - 3) + C_6(I_3), \tag{2.6}$$

where Σ is the strain energy function, I_i are the principal invariants of $\mathbf{B}$, C_i, $i = 1, \ldots, 5$, are the material constants, and $C_6(I_3)$ is an arbitrary function of I_3 that vanishes in the undeformed state where $I_1 = I_2 = 3$, $I_3 = 1$. In particular, if $C_3 = C_4 = C_5 = 0$ and the material is incompressible, it defines the Mooney-Rivlin material (2.5). In this work, we shall consider the special case of an incompressible material in which $C_6 = 0$. Then, the response functions β_1 and β_{-1} can be obtained as

$$\beta_1 = 2\frac{\partial \Sigma}{\partial I_1} = 2C_1 + 4C_3(I_1 - 3) + 2C_5(I_2 - 3), \tag{2.7}$$

$$\beta_{-1} = -2\frac{\partial \Sigma}{\partial I_2} = -2C_2 - 4C_4(I_2 - 3) - 2C_5(I_1 - 3). \tag{2.8}$$

3. Kinematics of the motion

We consider a rigid circular disk of mass M resting on a smooth inclined surface making an angle γ to the horizontal and supported symmetrically between identical, prestretched rubber cylinders of original length L, radius R_0, and surface area $A = \pi R_0^2$. The springs, prestretched an amount λ_s, are bonded to the disk at one end and to rigid supports at the other, as shown in Fig. 3.1. We suppose that each cylinder executes a combined ideal, time-dependent pure torsion deformation of amount $H(t)$ and simple shearing deformation of amount $K(t)$ superimposed on the longitudinal static stretch λ_s. Certainly, simple shear is an ideal deformation. Though bending will occur with the shearing, we shall ignore the bending effect for mathematical simplicity. We consider an incompressible material characterized by (2.4). To describe the motion, we shall break the combined shear-torsional motion into two steps. First, the body with a typical particle at (R, Θ, Z) undergoes a torsional deformation superimposed on the static longitudinal prestretch λ_s where the angle of twist of each cylinder is $H(t)$ per unit length. The particle is then moved to (r, θ, z). To effectively describe the simple shear deformation,

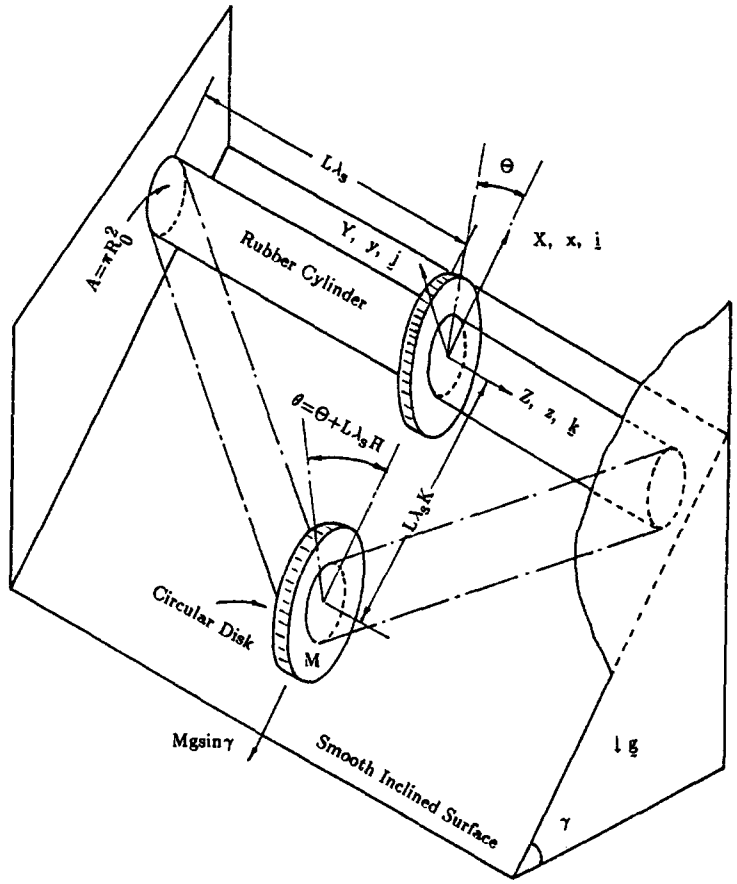

Fig. 3.1. A circular disk supported symmetrically between identical incompressible elastic rubber cylinders subjected to an initial longitudinal stretch λ_s.

we transform the cylindrical coordinates (r, θ, z) into rectangular coordinates (X, Y, z). Then the body undergoes an ideal, time-dependent simple shearing deformation of amount $K(t)$ superimposed on the torsional motion of $H(t)$. The final position of the particle of the body is then located at (x, y, z). Mathematically, the coupled shear-torsional motion is defined by the following equations relating (R, Θ, Z) and (x, y, z):

$$\begin{aligned} &r = \lambda_s^{-1/2} R, && X = r\cos\theta, && x = X + K(t)z, \\ &\theta = \Theta + H(t)\lambda_s Z, && Y = r\sin\theta, && y = Y, \\ &z = \lambda_s Z, && z = z, && z = z. \end{aligned} \tag{3.1}$$

Let **i**, **j**, and **k** denote the usual rectangular Cartesian basis in the directions of x, y, z, respectively, as shown in Fig. 3.1. Hence, by (3.1) and (2.3) and using the symbol $\otimes$ for the tensor product we find

$$\mathbf{F} = \lambda_s^{-1/2} \cos\theta(\mathbf{i}\otimes\mathbf{i} + \mathbf{j}\otimes\mathbf{j}) + \lambda_s \mathbf{k}\otimes\mathbf{k} + \lambda_s^{-1/2} \sin\theta(\mathbf{j}\otimes\mathbf{i} - \mathbf{i}\otimes\mathbf{j})$$
$$+ \lambda_s(K - Hr\sin\theta)\mathbf{i}\otimes\mathbf{k} + \lambda_s Hr\cos\theta\,\mathbf{j}\otimes\mathbf{k}, \tag{3.2}$$

$$\mathbf{B} = (\lambda_s^{-1} + K^2\lambda_s^2 - 2\lambda_s^2 KHr\sin\theta + \lambda_s^2 H^2 r^2 \sin^2\theta)\mathbf{i}\otimes\mathbf{i}$$
$$+ (\lambda_s^{-1} + \lambda_s^2 H^2 r^2 \cos^2\theta)\mathbf{j}\otimes\mathbf{j} + \lambda_s^2 \mathbf{k}\otimes\mathbf{k}$$
$$+ (K - Hr\sin\theta)\lambda_s^2 Hr\cos\theta(\mathbf{i}\otimes\mathbf{j} + \mathbf{j}\otimes\mathbf{i})$$
$$+ (K - Hr\sin\theta)\lambda_s^2(\mathbf{i}\otimes\mathbf{k} + \mathbf{k}\otimes\mathbf{i})$$
$$+ \lambda_s^2 Hr\cos\theta(\mathbf{j}\otimes\mathbf{k} + \mathbf{k}\otimes\mathbf{j}), \tag{3.3}$$

$$\mathbf{B}^{-1} = \lambda_s(\mathbf{i}\otimes\mathbf{i} + \mathbf{j}\otimes\mathbf{j}) + \lambda_s(\lambda_s^{-3} + K^2 + H^2r^2 - 2KHr\sin\theta)\mathbf{k}\otimes\mathbf{k}$$
$$- \lambda_s(K - Hr\sin\theta)(\mathbf{i}\otimes\mathbf{k} + \mathbf{k}\otimes\mathbf{i}) - \lambda_s Hr\cos\theta(\mathbf{j}\otimes\mathbf{k} + \mathbf{k}\otimes\mathbf{j}). \tag{3.4}$$

The principal invariants follow from these relations. We find

$$I_1(\mathbf{B}) = \lambda_s^2 + 2\lambda_s^{-1} + K^2\lambda_s^2 + \lambda_s^2 H^2 r^2 - 2\lambda_s^2 KHr\sin\theta, \tag{3.5}$$

$$I_2(\mathbf{B}) = \lambda_s^{-2} + 2\lambda_s + K^2\lambda_s + \lambda_s H^2 r^2 - 2\lambda_s KHr\sin\theta, \tag{3.6}$$

$$I_3(\mathbf{B}) = 1. \tag{3.7}$$

4. Cauchy sress components of the deformation

By the previous relations, equation (2.4) yields the following Cauchy stress components:

$$T_{11} = -p + \beta_1[\lambda_s^{-1} + K^2\lambda_s^2 - 2\lambda_s^2 KHr\sin\theta + \lambda_s^2 H^2 r^2 \sin^2\theta] + \beta_{-1}\lambda_s, \tag{4.1}$$

$$T_{22} = -p + \beta_1[\lambda_s^{-1} + \lambda_s^2 H^2 r^2 \cos^2\theta] + \beta_{-1}\lambda_s, \tag{4.2}$$

$$T_{33} = -p + \beta_1\lambda_s^2 + \beta_{-1}[\lambda_s(\lambda_s^{-3} + K^2 + H^2r^2 - 2KHr\sin\theta)], \tag{4.3}$$

$$T_{12} = T_{21} = \beta_1[(K - Hr\sin\theta)\lambda_s^2 Hr\cos\theta], \tag{4.4}$$

$$T_{13} = T_{31} = \lambda_s(K - Hr\sin\theta)[\lambda_s\beta_1 - \beta_{-1}], \tag{4.5}$$

$$T_{23} = T_{32} = \lambda_s Hr\cos\theta[\lambda_s\beta_1 - \beta_{-1}]. \tag{4.6}$$

Equations (4.1), (4.3), and (4.5) yield the following relation between $T_{11} - T_{33}$ and T_{13}:

$$T_{11} - T_{33} = \frac{\lambda_s^{-3} - 1 + K^2 - 2KHr\sin\theta + H^2r^2\sin^2\theta}{K - Hr\sin\theta} \times T_{13} - \beta_{-1}\lambda_s H^2r^2\cos^2\theta. \tag{4.7}$$

Hence, when $H = 0$, equation (4.7) yields the famous universal relation in simple shear. On the other hand, when $\beta_{-1} = 0$, equation (4.7) reduces to

$$T_{11} - T_{33} = \frac{\lambda_s^{-3} - 1 + K^2 - 2KHr\sin\theta + H^2r^2\sin^2\theta}{K - Hr\sin\theta} T_{13}. \tag{4.8}$$

This is a universal relation for all incompressible elastic materials with $\beta_{-1} = 0$ and is independent of the response function β_1.

There exist two additional universal relations. They can be easily identified from (4.1) through (4.6) and are given by

$$\frac{T_{13}}{T_{23}} = \frac{K}{Hr\cos\theta} - \tan\theta, \tag{4.9}$$

$$T_{11} - T_{22} = \frac{K^2 - 2KHr\sin\theta - H^2r^2\cos 2\theta}{(K - Hr\sin\theta)Hr\cos\theta} T_{12}. \tag{4.10}$$

These two universal relations can also be obtained directly from tensor equations $\mathbf{TB} = \mathbf{BT}$ and $\mathbf{TB}^{-1} = \mathbf{B}^{-1}\mathbf{T}$ developed by Beatty [7]. Each of these two tensor equations yields three scalar equations expressed in terms of the physical components T_{ij} and B_{ij}. Among these equations, two are the generators of the universal relations (4.9) and (4.10). They are

$$B_{12}^{-1}(T_{11} - T_{22}) = (B_{11}^{-1} - B_{22}^{-1})T_{12} + B_{13}^{-1}T_{32} - T_{13}B_{32}^{-1}, \tag{4.11}$$

for relation (4.9), and

$$B_{12}(T_{11} - T_{22}) = (B_{11} - B_{22})T_{12} + B_{13}T_{32} - T_{13}B_{32}, \tag{4.12}$$

for relation (4.10).

The traction on the surface of the cylinder where the circular disk is bonded can be found as

$$\mathbf{t} = \mathbf{T}\mathbf{k} = T_{13}\mathbf{i} + T_{23}\mathbf{j} + T_{33}\mathbf{k}. \tag{4.13}$$

Hence, the force exerted on the surface by the disk is given by

$$\mathbf{N} = \int_{\mathscr{A}} \mathbf{t}\, \mathrm{d}\mathscr{A} = \mathbf{N}_1 + \mathbf{N}_2 + \mathbf{N}_3, \tag{4.14}$$

where the integral is evaluated over the deformed surface $\mathscr{A}$ connected with the disk and

$$\mathbf{N}_3 = \int_{\mathscr{A}} T_{33}\, \mathrm{d}\mathscr{A}\mathbf{k} \tag{4.15}$$

is the normal force in the z direction. This force is balanced through the symmetry of the spring-mass system shown in Fig. 3.1. $\mathbf{N}_2$ in (4.14) is the shear force in the y direction and is given by

$$\mathbf{N}_2 = \int_{\mathscr{A}} T_{23}\, \mathrm{d}\mathscr{A}\mathbf{j} = \int_0^{2\pi} \int_0^{r_0} \lambda_s H r \cos\theta [\lambda_s \beta_1 - \beta_{-1}]\, \mathrm{d}\theta r\, \mathrm{d}r\mathbf{j}, \tag{4.16}$$

where r_0 is the radius of the deformed surface $\mathscr{A}$ and is related to R_0 by $r_0 = \lambda_s^{-1/2} R_0$. Similarly, the shear force $\mathbf{N}_1$ in the x direction is given by

$$\mathbf{N}_1 = \int_{\mathscr{A}} T_{13}\, \mathrm{d}\mathscr{A}\mathbf{i} = \int_0^{2\pi} \int_0^{r_0} \lambda_s (K - Hr \sin\theta)[\lambda_s \beta_1 - \beta_{-1}]\, \mathrm{d}\theta r\, \mathrm{d}r\mathbf{i}. \tag{4.17}$$

Moreover, the torque $\mathbf{M}$ on the bonding surface in the z direction due to the traction is found to be

$$\begin{aligned}\mathbf{M} &= \int_{\mathscr{A}} (xT_{23} - yT_{13})\, \mathrm{d}\mathscr{A}\mathbf{k} \\ &= \int_0^{2\pi} \int_0^{r_0} [(r\cos\theta + Kz)\lambda_s H r \cos\theta(\lambda_s\beta_1 - \beta_{-1}) \\ &\quad - r\sin\theta\lambda_s(K - Hr\sin\theta)(\lambda_s\beta_1 - \beta_{-1})]\, \mathrm{d}\theta r\, \mathrm{d}r\mathbf{k}.\end{aligned} \tag{4.18}$$

5. Formulation of the motion of the disk

We shall consider the motion of the disk in two aspects: the motion of the center of the disk and the rotational motion of the disk about its center. By (3.1), the acceleration of the center of the disk and the angular acceleration of the disk about its center are found as

$$\mathbf{a} = \lambda_s L\ddot{K}\mathbf{i}, \quad \ddot{\theta} = \lambda_s L\ddot{H}, \tag{5.1}$$

where L is the original length of the cylinder. Hence, the motion of the disk is governed by

$$M\mathbf{a} = Mg^*\mathbf{i} - 2\mathbf{N}_1, \quad I\ddot{\theta}\mathbf{k} = -2\mathbf{M}, \tag{5.2}$$

where M and I are respectively the mass and the moment of inertia of the disk and

$$g^* = g \sin\gamma \tag{5.3}$$

in which g is the gravitational acceleration. Let R_g be the radius of gyration of the disk. Then,

$$I = MR_g^2. \tag{5.4}$$

6. Motions of an oscillator with constant β_1 and β_{-1}

We now consider a special class of materials whose response functions β_1 and β_{-1} are constants independent of both time t and position $\mathbf{x}$, such as the Mooney-Rivlin materials. In this case, we find from (4.16) and (4.17)

$$\mathbf{N}_2 = \mathbf{0}, \quad \mathbf{N}_1 = A[\lambda_s\beta_1 - \beta_{-1}]K\mathbf{i}. \tag{6.1}$$

For constant response functions β_1 and β_{-1}, equation (4.18) reduces to

$$\mathbf{M} = \tfrac{1}{2}AR_0^2\lambda_s^{-1}[\lambda_s\beta_1 - \beta_{-1}]H\mathbf{k}. \tag{6.2}$$

Hence, the equations of motion of the disk are obtained from the previous relations and are given by

$$\ddot{K} + \omega_K^2 K = \frac{g^*}{L\lambda_s}, \tag{6.3}$$

$$\ddot{H} + \omega_H^2 H = 0, \tag{6.4}$$

where

$$\omega_K = \sqrt{\frac{2A}{ML\lambda_s}[\lambda_s\beta_1 - \beta_{-1}]}, \tag{6.5}$$

$$\omega_H = \sqrt{\frac{A}{ML}d^2\lambda_s^{-2}[\lambda_s\beta_1 - \beta_{-1}]}, \tag{6.6}$$

with the gyration ratio d defined by

$$d \equiv \frac{R_0}{R_g}. \tag{6.7}$$

Hence, for this particular class of materials, the motion of the disk is governed by two independent linear differential equations. The equilibrium position can be easily established from (6.3) through (6.6), and the static shear deflection K_s and static torsion H_s are given by

$$K_s = \frac{Mg^*}{2A(\lambda_s\beta_1 - \beta_{-1})}, \quad H_s = 0. \tag{6.8}$$

Hence, the solutions to (6.3) and (6.4) are simple harmonic. The ratio of the frequencies given by (6.5) and (6.6) is found to be

$$\frac{\omega_H}{\omega_K} = \frac{d}{\sqrt{2\lambda_s}}. \tag{6.9}$$

Thus, the frequency ratio (6.9) is a universal relation for every incompressible elastic shaft with constant response functions β_1 and β_{-1}. The only design parameter is the gyration ratio d. The frequency ratio is a monotone decreasing function of the axial stretch λ_s. It approaches infinity when $\lambda_s \to 0$ and approaches 0 as $\lambda_s \to \infty$. The frequency ratio ω_H/ω_K reaches 1 when $d = \sqrt{2\lambda_s}$. Hence, when $d > (<)\sqrt{2\lambda_s}$, the torsional oscillation vibrates faster (slower) than the shearing oscillation. The position $d = \sqrt{2\lambda_s}$ is the point where both vibrate at the same speed.

Bearing in mind the equilibrium position (6.8), the closed form solutions to (6.3) and (6.4) are simple harmonic and can be written as

$$K = K_s + K_0 \cos(\omega_K t + \theta_{K0}), \tag{6.10}$$

$$H = H_0 \cos(\omega_H t + \theta_{H0}), \tag{6.11}$$

where K_s is the static equilibrium shear deflection determined by (6.8) and K_0, H_0, θ_{K0}, and θ_{H0} are constants determined by the initial conditions.

To understand the dependence of the circular frequency ω_K and ω_H on the longitudinal static stretch λ_s, we shall look at two special cases: (1) the motion on an inclined surface; and (2) the motion on a horizontal surface.

6.1. *The motions on a smooth inclined surface* ($\gamma \neq 0$)

For the motion of the disk on a smooth inclined surface with $\gamma \neq 0$, we can remove the mass in relations (6.5) and (6.6) by the equilibrium condition (6.8). Hence, we find

$$\omega_K = p_0\sqrt{\frac{1}{K_s\lambda_s}}, \quad \omega_H = p_0 d\sqrt{\frac{1}{2K_s\lambda_s^2}}, \quad p_0 \equiv \sqrt{\frac{g^*}{L}}, \quad \text{with } \frac{\omega_K}{\omega_H} = \frac{\sqrt{2\lambda_s}}{d}. \tag{6.12}$$

Hence, the frequency ratio between shearing and torsion is a universal relation independent of the material constants β_1 and β_{-1}. Both frequencies are decreasing functions of λ_s and K_s. Relations in (6.12), of course, have been obtained separately on numerous occasions.

6.2. *The horizontal motion*

For motion on a horizontal surface for which $\gamma = 0°$, we have $K_s = 0$ because $g^* = 0$. For the Mooney-Rivlin model (2.5), the frequencies (6.5) and (6.6) reduce to

$$\frac{\omega_K}{\omega_0} = \sqrt{\frac{2(\lambda_s+\alpha)}{\lambda_s(1+\alpha)}}, \quad \frac{\omega_H}{\omega_0} = d\sqrt{\frac{(\lambda_s+\alpha)}{\lambda_s^2(1+\alpha)}}, \quad \omega_0 \equiv \sqrt{\frac{AG}{ML}}. \tag{6.13}$$

When $\alpha = 0$, the normalized frequency $\omega_K/\omega_0 = \sqrt{2}$. Hence, the frequency of finite amplitude shearing vibrations of a neo-Hookean oscillator is a constant and this constant frequency is not affected by the longitudinal stretch λ_s. For other cases, the frequencies approach infinity as $\lambda_s \to 0$. When $\lambda_s \to \infty$, $\omega_H/\omega_0 \to 0$ while $\omega_K/\omega_0 \to \sqrt{2/(1+\alpha)}$ (Fig. 6.1). For the level oscillation with $\lambda_s = 1$, we find from (6.13) $\omega_K/\omega_0 = \sqrt{2}$, $\omega_H/\omega_0 = d$. These frequency responses are independent of the material parameter α. Hence, by level oscillation, one cannot tell one Mooney-Rivlin material from the other.

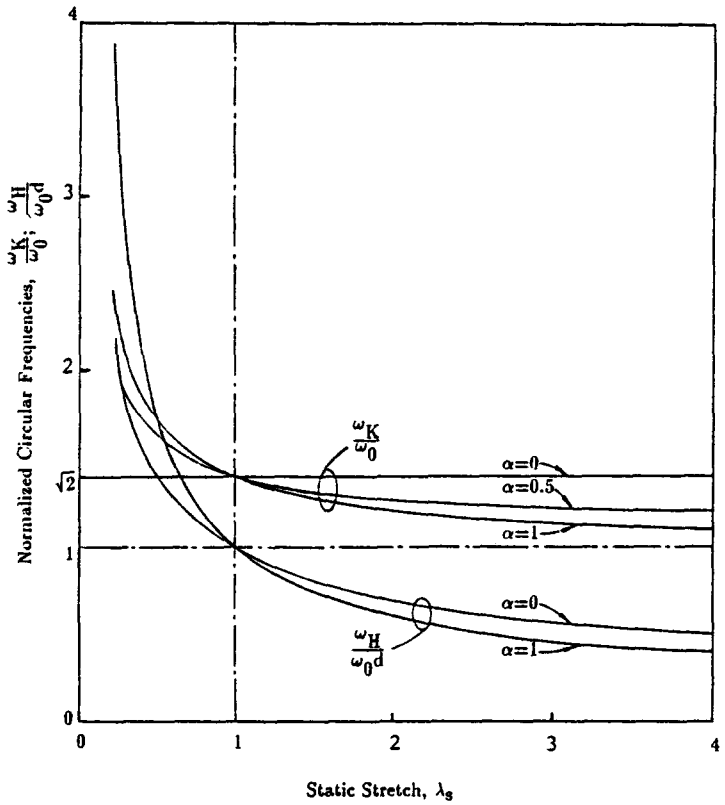

Fig. 6.1. Normalized circular frequencies versus static stretch λ_s for coupled shearing torsional motions of a circular disk supported by Mooney-Rivlin rubber cylinders for various values of α.

7. Equations of motion of the disk supported by quadratic springs

The material response functions for quadratic material are characterized by (2.7) and (2.8). By (2.7), (2.8), (3.5), and (3.6) we find

$$\lambda_s\beta_1 - \beta_{-1} = q_0 + q_1(K^2 + H^2r^2 - 2KHr\sin\theta), \tag{7.1}$$

where q_0 and q_1 are constants given by

$$q_0 = 2(\lambda_s C_1 + C_2) + (4\lambda_s C_3 + 2C_5)(\lambda_s^2 + 2\lambda_s^{-1} - 3)$$
$$+ (4C_4 + 2\lambda_s C_5)(\lambda_s^{-2} + 2\lambda_s - 3), \tag{7.2}$$

$$q_1 = (4\lambda_s C_3 + 2C_5)\lambda_s^2 + (4C_4 + 2\lambda_s C_5)\lambda_s. \tag{7.3}$$

Using (7.1) in (4.16), (4.17), and (4.18) we find

$$\mathbf{N}_2 = \mathbf{0}, \quad \mathbf{N}_1 = A(q_0 K + q_1 K^3 + R_0^2 \lambda_s^{-1} q_1 K H^2)\mathbf{i}, \tag{7.4}$$

$$\mathbf{M} = \frac{AR_0^2}{2\lambda_s^2}(\lambda_s q_0 H + \tfrac{2}{3} R_0^2 q_1 H^3 + 2\lambda_s q_1 H K^2)\mathbf{k}. \tag{7.5}$$

Hence, the equations of motion of the disk are obtained from (5.1) and (5.2):

$$\ddot{K} + \frac{2Aq_0}{ML\lambda_s} K + \frac{2Aq_1}{ML\lambda_s} K^3 + \frac{2AR_0^2 q_1}{ML\lambda_s^2} K H^2 = \frac{g^*}{L\lambda_s}, \tag{7.6}$$

$$\ddot{H} + \frac{Aq_0 d^2}{ML\lambda_s^2} H + \frac{2AR_0^2 d^2 q_1}{3ML\lambda_s^3} H^3 + \frac{2Ad^2 q_1}{ML\lambda_s^2} H K^2 = 0, \tag{7.7}$$

If q_0 and q_1 are positive, all the coefficients in equations (7.6) and (7.7) are positive. Hence, the nonlinear differential equations (7.6) and (7.7) describe the motion of the disk supported by the "hard spring". We shall assume this is the case throughout this work. The coefficients of the nonlinear terms in equations (7.6) and (7.7) are all proportional to the material constant q_1. When $q_1 = 0$, the equations of motion (7.6) and (7.7) reduce to two independent linear differential equations whose solutions are simple harmonic.

We now introduce

$$\hat{t} \equiv t\sqrt{\frac{Aq_0}{ML}}, \tag{7.8}$$

to reduce equations (7.6) and (7.7) to

$$K'' + \omega_K^2 K + \varepsilon_K K^3 + \mu_K K H^2 = \hat{g}, \tag{7.9}$$

$$H'' + \omega_H^2 H + \varepsilon_H H^3 + \mu_H H K^2 = 0, \tag{7.10}$$

where

$$K'' \equiv \frac{\mathrm{d}^2 K}{\mathrm{d}\hat{t}^2}, \quad H'' \equiv \frac{\mathrm{d}^2 H}{\mathrm{d}\hat{t}^2}, \tag{7.11}$$

$$\omega_K = \sqrt{\frac{2}{\lambda_s}}, \quad \varepsilon_K = \frac{2\beta}{\lambda_s}, \quad \mu_K = \frac{2\beta R_0^2}{\lambda_s^2}, \tag{7.12}$$

$$\omega_H = \frac{d}{\lambda_s}, \quad \varepsilon_H = \frac{2\beta d^2 R_0^2}{3\lambda_s^3}, \quad \mu_H = \frac{2\beta d^2}{\lambda_s^2}, \tag{7.13}$$

$$\beta \equiv \frac{q_1}{q_0}, \quad \hat{g} \equiv \frac{Mg^*}{Aq_0\lambda_s}. \tag{7.14}$$

In this work, we shall use the prime $'$ to denote the derivative with respect to the normalized time $\hat{t}$ and assume that q_1 is very small compared with q_0. Hence, the ratio $\beta = q_1/q_0$ defined in $(7.14)_1$ is a small parameter. We shall use it later for the stability analysis by the perturbation method. On the other hand, when H and K are small, we may drop all nonlinear terms in (7.9) and (7.10) to linearize the equations in studying small amplitude vibrations of the disk. In this case, equations reduce to (6.3) and (6.4) whose solutions are simple harmonic. Hence, the conclusion about the small oscillation in this case is obvious. We shall not pursue its detailed discussion here and rather focus our study on the stability properties of the coupled motion between shearing and torsion for the following two special cases: (1) small shearing superimposed on the finite torsion; and (2) small torsion superimposed on the finite shearing.

8. Stability of small shearing superimposed on finite torsion

We start this chapter with the study of small shearing superimposed on the finite torsion. In this case, by dropping the nonlinear terms in K, the equations of motion (7.9) and (7.10) reduce to

$$K'' + \omega_K^2 K + \mu_K K H^2 = \hat{g}, \tag{8.1}$$

$$H'' + \omega_H^2 H + \varepsilon_H H^3 = 0. \tag{8.2}$$

It is clear that (8.2) is Duffing's equation whose solution is periodic. This solution may be written in terms of the elliptic integral which is derived below.

Since the system for H is conservative and the solution to (8.2) is a periodic function with equilibrium position $H_s = 0$ as its center, every initial value problem with (H_0, H_0') is equivalent to the problem in which the mass is released from rest at either of its extreme positions. Hence, we may assume without loss of generality the initial condition of $(H_0, 0)$. In this case, by multiplying H' on each side of (8.2) we obtain

$$H''H' + \omega_H^2 HH' + \varepsilon_H H^3 H' = 0. \tag{8.3}$$

This equation is integrated into

$$(H')^2 + \omega_H^2 H^2 + \tfrac{1}{2}\varepsilon_H H^4 = C. \tag{8.4}$$

The integration constant C may be obtained from the initial condition of $(H_0, 0)$ and is given by

$$C = \omega_H^2 H_0^2 + \tfrac{1}{2}\varepsilon_H H_0^4. \tag{8.5}$$

Substituting (8.5) into (8.4) we find

$$(H')^2 = (H_0^2 - H^2)[\omega_H^2 + \tfrac{1}{2}\varepsilon_H (H_0^2 + H^2)]. \tag{8.6}$$

At this point, we use the transformation

$$H = H_0 \cos\phi \tag{8.7}$$

to change (8.6) into

$$(\phi')^2 = \omega_H^2 + \varepsilon_H H_0^2 - \tfrac{1}{2}\varepsilon_H H_0^2 \sin^2\phi. \tag{8.8}$$

Bearing in mind the initial condition of $(H_0, 0)$ and transformation (8.7), equation (8.8) can be integrated into

$$\hat{t} = \pm\frac{1}{v}\int_0^{\phi} \frac{\mathrm{d}\psi}{\sqrt{1 - k^2 \sin^2\psi}} = \pm\frac{1}{v} F(\phi, k), \tag{8.9}$$

where

$$\begin{aligned} v &= \sqrt{\omega_H^2 + \varepsilon_H H_0^2} = \frac{d}{\lambda_s}\sqrt{1 + \frac{2\beta R_0^2 H_0^2}{3\lambda_s}}, \\ k &= \sqrt{\frac{\varepsilon_H H_0^2}{2(\omega_H^2 + \varepsilon_H H_0^2)}} = \sqrt{\frac{1}{2 + \dfrac{3\lambda_s}{\beta R_0^2 H_0^2}}}, \end{aligned} \tag{8.10}$$

and $F(\phi, k)$ is the elliptic integral of the first kind. The period of the finite amplitude oscillations is determined by

$$\tau = \frac{4}{v} F\left(\frac{\pi}{2}, k\right) = \tau^* \frac{2F\left(\dfrac{\pi}{2}, k\right)}{\pi\sqrt{1 + \dfrac{\varepsilon_H H_0^2}{\omega_H^2}}} = \tau^* \frac{2F\left(\dfrac{\pi}{2}, k\right)}{\pi\sqrt{1 + \dfrac{2\beta R_0^2 H_0^2}{3\lambda_s}}}, \tag{8.11}$$

in which $F(\pi/2, k)$ is the complete elliptic integral of the first kind and

$\tau^* \equiv 2\pi/\omega_H$ is the period of the corresponding linear oscillator. We notice from (8.11) that the period of the finite amplitude oscillations depends on the initial condition H_0 through k. This is a unique characteristic of nonlinear vibrations. For infinitesimal oscillation in which $\varepsilon_H = 0$, we find from (8.10) that $k = 0$, $v = \omega_H$. Hence, we obtain by (8.11)

$$\tau = \frac{4}{\omega_H} F\left(\frac{\pi}{2}, 0\right) = \frac{4}{\omega_H}\frac{\pi}{2} = \frac{2\pi}{\omega_H} = \tau^*. \tag{8.12}$$

Hence, the frequency of infinitesimal vibration is independent of the initial H_0. This result, of course, can be easily obtained from the analysis of linear vibration. For the nonlinear oscillator, we may recall (8.10) for k and find that the normalized period τ/τ^* in (8.11) depends on the physical parameters β, λ_s, and R_0H_0 alone. This dependence is more clearly demonstrated through Fig. 8.1 where τ/τ^* is shown as a function of R_0H_0 under different static stretch λ_s for the case of $\beta = 0.5$. It is obvious that the normalized period is a decreasing

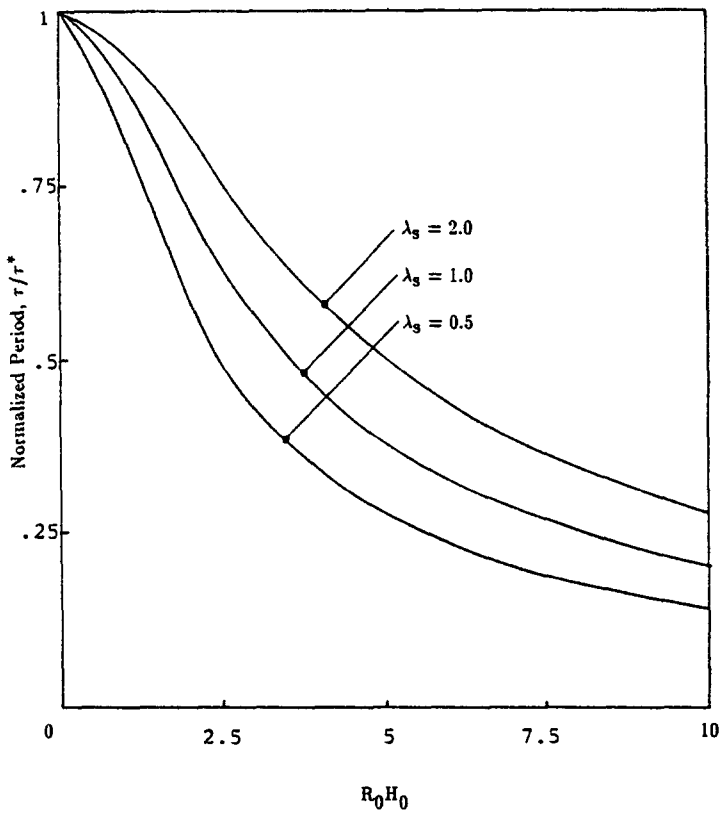

Fig. 8.1. Dimensionless period as a function of the initial value R_0H_0 for finite amplitude torsional motions of a quadratic oscillator for material ratio $\beta = 0.5$ and for selected values of λ_s.

function of R_0H_0. When $R_0H_0 \to 0$, the nonlinear oscillator achieves its maximum period of τ^*. Hence, the frequency of the nonlinear oscillator is always greater than that of the linear oscillator. In the mean time, for each given R_0H_0, the normalized period is an increasing function of the static stretch λ_s. The dependence of τ/τ^* for other values of β is shown in Fig. 8.2 and Fig. 8.3 with $\beta = 0.05$ and 1.0 respectively. τ/τ^* as a decreasing function of β is shown in Fig. 8.3+.

Solution (8.9) also may be written in terms of the Jacobian function

$$\phi = \pm \operatorname{sn} v\hat{t} = \pm \operatorname{sn}(v\hat{t}, k), \tag{8.13}$$

where sn x is the Jacobian elliptic function associated with the elliptic integral of the first kind. It is a periodic function with period of $4F(\pi/2, k)$. Hence, the solution for torsion H to equation (8.2) is finally obtained as

$$H = H_0 \cos[\operatorname{sn}(v\hat{t}, k)]. \tag{8.14}$$

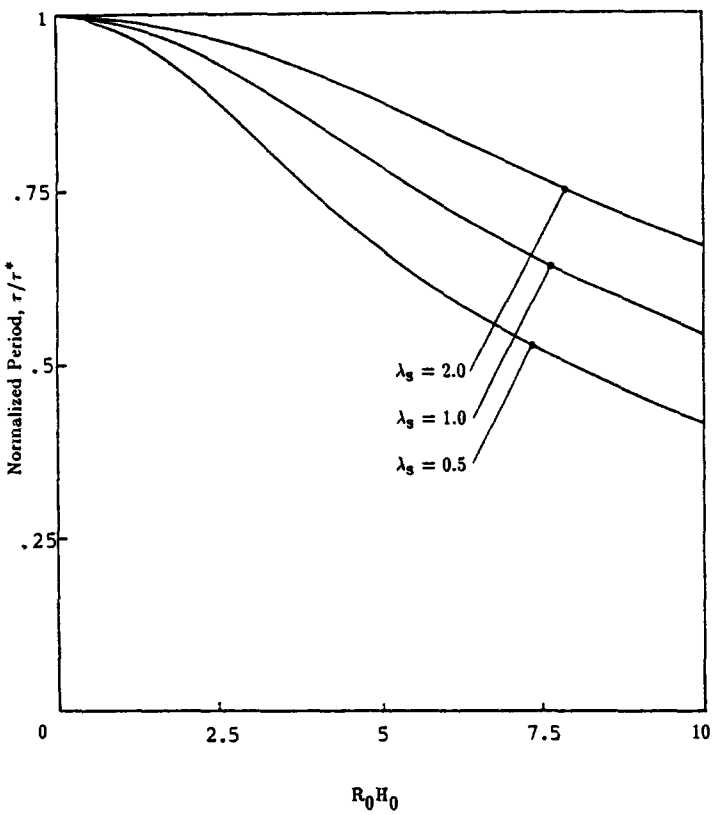

Fig. 8.2. Dimensionless period as a function of the initial value R_0H_0 for finite amplitude torsional motions of a quadratic oscillator for material ratio $\beta = 0.05$ and for selected values of λ_s.

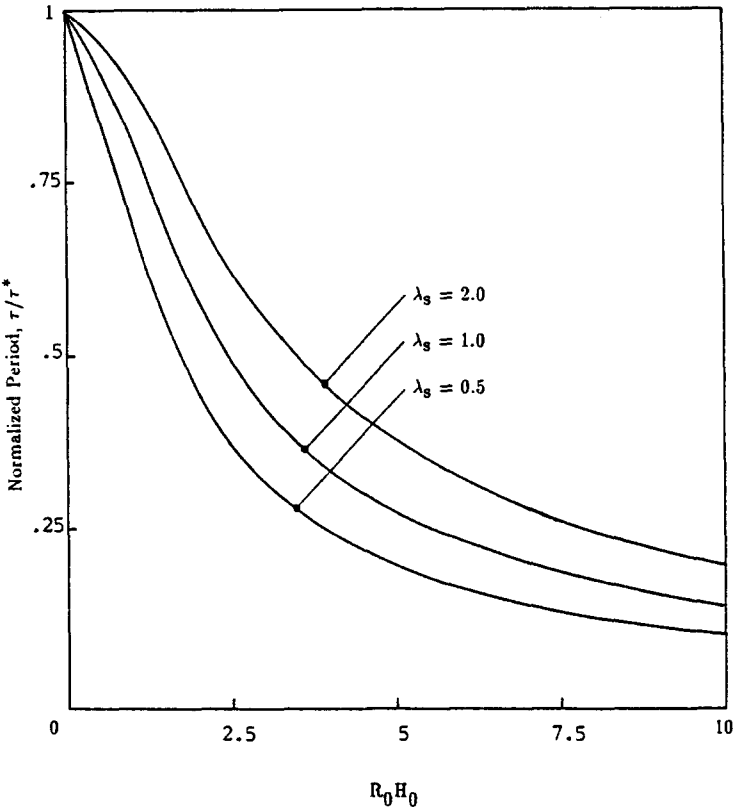

Fig. 8.3. Dimensionless period as a function of the initial value R_0H_0 for finite amplitude torsional motions of a quadratic oscillator for material ratio $\beta = 1.0$ and for selected values of λ_s.

Hence, the solution H is a periodic function with period $\tau = (4/v)F(\pi/2, k)$. The phase diagrams of this motion are shown in Fig. 8.4 for various initial conditions. The motion is symmetric about its equilibrium position located at the origin. Figure 8.5 is the phase diagrams of the motion under various values of static stretch λ_s. As λ_s increases, the speed $H'(\hat{t})$ decreases and hence the longer period, an expected property since τ/τ^* is an increasing function of λ_s. The phase diagrams of the motion for different values of β are shown in Fig. 8.6. When β increases, the speed $H'(\hat{t})$ increases and hence the shorter period, another expected property since τ/τ^* is a decreasing function of β. We have seen that the normalized period of the motion is independent of the gyration ratio d. However, the motion itself depends on d since ω_H is a function of d as shown in (7.13). The phase diagrams of torsional motion for various values of d are shown in Fig. 8.7. We see that larger d produces higher speed and hence greater frequency or smaller period.

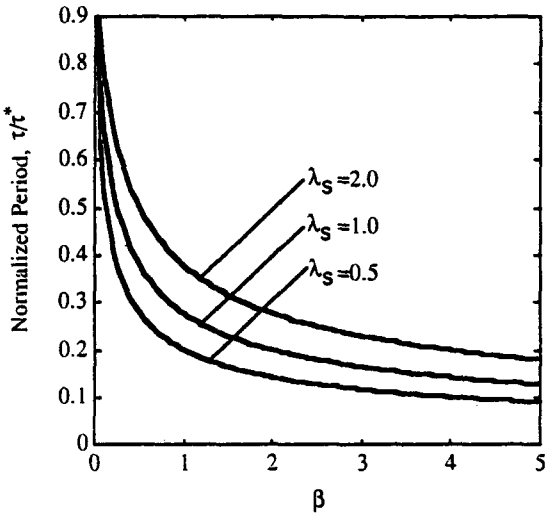

Fig. 8.3+. Dimensionless period as a function of the material ratio β for finite amplitude torsional motions of a quadratic oscillator for initial value $R_0H_0 = 5$ and for selected values of λ_s.

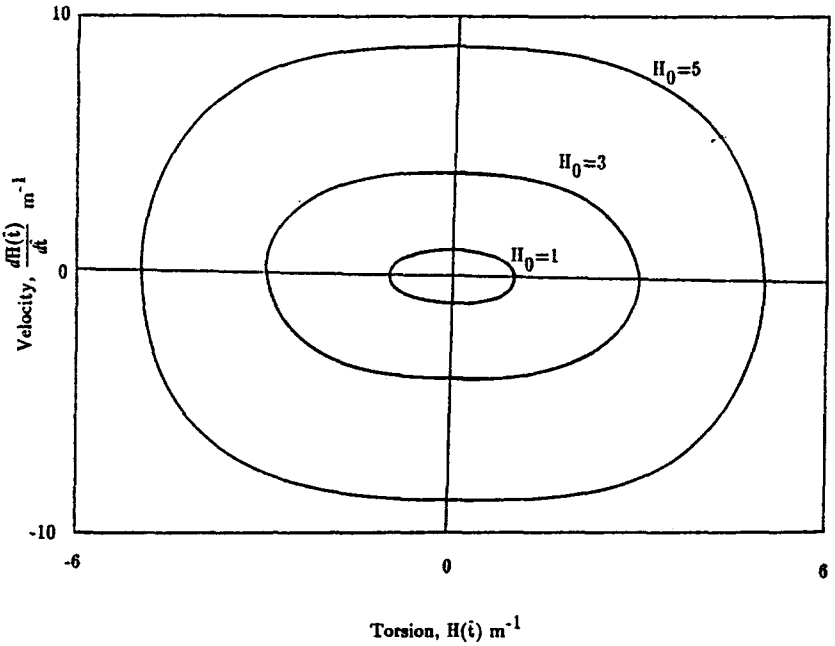

Fig. 8.4. Phase plane diagrams of the finite amplitude torsional motions of a quadratic oscillator for $R_0 = 0.5m$, $\beta = 0.5$, $\lambda_s = 0.5$, $d = 0.5$ and for selected values of the initial data $(H_0, 0)$.

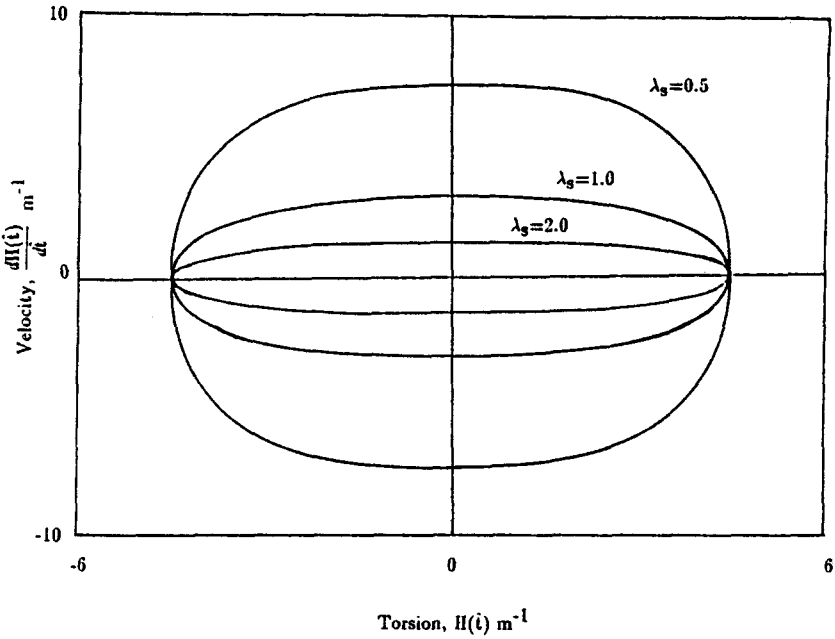

Fig. 8.5. Phase plane diagrams of the finite amplitude torsional motions of a quadratic oscillator for $R_0 = 0.5m$, $\beta = 0.5$, $d = 0.5$, $H_0 = 4.5\ \mathrm{m}^{-1}$ and for selected values of λ_s.

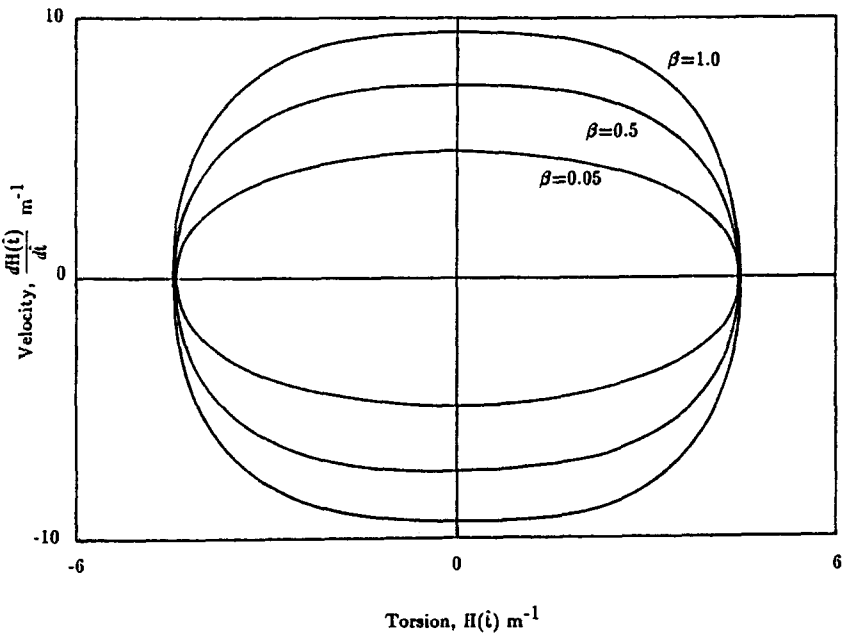

Fig. 8.6. Phase plane diagrams of the finite amplitude torsional motions of a quadratic oscillator for $R_0 = 0.5$ m, $\lambda_s = 0.5$, $d = 0.5$, $H_0 = 4.5\ \mathrm{m}^{-1}$ and for selected values of β.

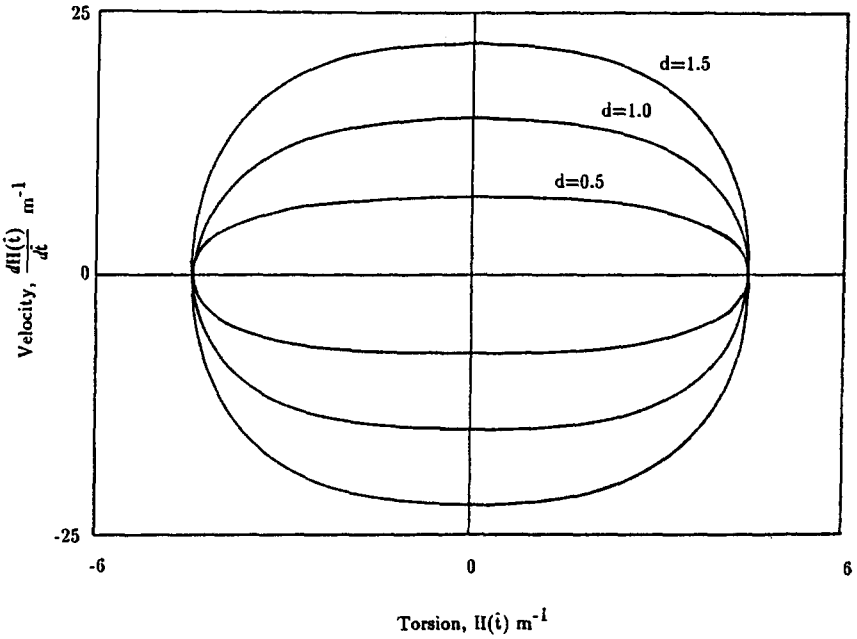

Fig. 8.7. Phase plane diagrams of the finite amplitude torsional motions of a quadratic oscillator for $R_0 = 0.5m$, $\beta = 0.5$, $\lambda_s = 0.5$, $H_0 = 4.5\ \mathrm{m}^{-1}$ and for selected values of d.

By using (8.14) in (8.1) we find the equation for small shearing as

$$K'' + \{a + q\cos[2\,\mathrm{sn}(v\hat{t}, k)]\}K = \hat{g}, \tag{8.15}$$

where

$$a \equiv \omega_K^2 + \tfrac{1}{2}\mu_K H_0^2, \quad q \equiv \tfrac{1}{2}\mu_K H_0^2. \tag{8.16}$$

Equation (8.15) is a special type of Hill's equation. To study its stability property, we proceed in two directions: (1) to study the stability of K for $\hat{t} \ll \tau$; and (2) to study the stability of K for the entire time region.

8.1. Small shearing with $\hat{t} \ll \tau$

The Taylor's series for the Jacobian elliptic function sn x is given by

$$\mathrm{sn}\,x = x - \frac{1+k^2}{3!}x^3 + \frac{1+14k^2+k^4}{5!}x^5 - \frac{1+135k^2+135k^4+k^6}{7!}x^7 + \cdots \tag{8.17}$$

for small x. If we keep the first term of (8.17) only as an approximation and use it in (8.15), we find

$$K'' + (a + q\cos 2v\hat{t})K = \hat{g}. \tag{8.18}$$

In this equation, k, as a function of ω_H, ε_H, and H_0 given by $(8.10)_2$, disappears. However, the stability property of K still depends on those parameters through v shown in $(8.10)_1$.

We now consider the transformation

$$z = 2v\hat{t} \tag{8.19}$$

in (8.18) to obtain

$$\frac{\mathrm{d}^2K}{\mathrm{d}z^2} + (\delta + \varepsilon\cos z)K = b^*, \tag{8.20}$$

where

$$\delta \equiv \frac{a}{4v^2}, \quad \varepsilon \equiv \frac{q}{4v^2}, \quad b^* \equiv \frac{\hat{g}}{4v^2}. \tag{8.21}$$

We shall now consider two special cases: (1) the motion of the disk on a horizontal surface in which $\gamma = 0$; and (2) the motion of the disk on an inclined surface in which $\gamma \neq 0$. The stability of small shearing superimposed on the finite torsion will be studied for each case.

8.1.1. Motions on a horizontal surface

In this case, $\gamma = 0$ and bearing in mind relations $(7.14)_2$ and (5.3), equation (8.20) reduces to

$$\frac{\mathrm{d}^2K}{\mathrm{d}z^2} + (\delta + \varepsilon\cos z)K = 0. \tag{8.22}$$

Equation (8.22), which is in the same form as (4.1) in [8], is Mathieu's equation whose stability property has been studied extensively, and, in particular, as mentioned by Stoker [8], the stable and unstable regions in the δ, ε-plane have been determined completely for all values of δ and ε. This δ, ε-plane is the stability map which can be found from Fig. 4.1 in [8]. Hence, the stability of small shearing K in (8.22) is determined by computing δ and ε and then locating the point (δ, ε) in the map. We also find from (8.21), (8.16), and (7.12) that δ and ε are positive because q_0 and q_1 are assumed

to be positive. Hence, the stability of K is completely determined by Fig. 4.1 in [8].

It is also shown in [8] that for large values of ε the stable regions become very narrow. Hence, for large values of ε, the solution to (8.22) is more likely to become unstable. From (8.21), (8.16), (8.10), (7.12), and (7.13) we find

$$\delta = \frac{1}{d^2}\frac{6\lambda_s^2 + 3\lambda_s\beta R_0^2 H_0^2}{12\lambda_s + 8\beta R_0^2 H_0^2}, \quad \varepsilon = \frac{1}{4d^2\left[\dfrac{2}{3\lambda_s} + \dfrac{1}{\beta R_0^2 H_0^2}\right]}. \tag{8.23}$$

Obviously, ε depends on the longitudinal static stretch λ_s. However, its specific dependence on λ_s relies on the value of the material ratio $\beta \equiv q_1/q_0$ which is a function of λ_s by (7.2) and (7.3). Since we assume the material ratio β is small, ε is also small. This will make K more likely to be stable. For a given material in which β is a fixed constant, the dependence of ε on the initial torsion H_0 and the gyration ratio d is obvious in (8.23). We find that ε decreases as H_0 decreases. As $d = R_0/R_g$ increases, ε becomes smaller. Hence, *small initial torsion H_0 and small disk radius $R_d = \sqrt{2}R_g$, which produces small ε, tend to stabilize shearing motion for the disk on a horizontal surface with $\hat{t} \ll \tau$.* However, the exact stability property of K still depends on the location of (δ, ε) on the stability map.

8.1.2. Motions on an inclined surface ($\gamma \neq 0$)

In this case, the motion of small K is governed by (8.20). Problems like this are usually treated by the perturbation method. We shall first use this approach as outlined in [8] to study its stability property for small ε. When ε is small, we may assume that the solutions $K(z, \varepsilon)$ of (8.20) as well as $\delta(\varepsilon)$ can be expanded in series of powers of ε as follows:

$$K = K_0 + \varepsilon K_1 + \varepsilon^2 K_2 + \cdots, \tag{8.24}$$

$$\delta = \delta_0 + \varepsilon\delta_1 + \varepsilon^2\delta_2 + \cdots. \tag{8.25}$$

This small ε can be interpreted as a weak nonlinearity with small β. The relation between ε and β can be found in $(8.23)_2$. Inserting (8.24) and (8.25) in (8.20) yields the following relation:

$$\left(\frac{\mathrm{d}^2K_0}{\mathrm{d}z^2} + \varepsilon\frac{\mathrm{d}^2K_1}{\mathrm{d}z^2} + \varepsilon^2\frac{\mathrm{d}^2K_2}{\mathrm{d}z^2} + \cdots\right) + [(\delta_0 + \varepsilon\delta_1 + \varepsilon^2\delta_2 + \cdots) + \varepsilon\cos z]$$

$$\times (K_0 + \varepsilon K_1 + \varepsilon^2 K_2 + \cdots) = b^*. \tag{8.26}$$

To satisfy this equation, the following equations obtained by equating the coefficients of like powers of ε on both sides of (8.26) must hold:

$$\frac{d^2K_0}{dz^2} + \delta_0 K_0 = b^*, \tag{8.27}$$

$$\frac{d^2K_1}{dz^2} + \delta_0 K_1 = -\delta_1 K_0 - K_0 \cos z, \tag{8.28}$$

$$\frac{d^2K_2}{dz^2} + \delta_0 K_2 = -\delta_2 K_0 - \delta_1 K_1 - K_1 \cos z. \tag{8.29}$$

. . . . . .

Hence, we find from (8.27)

$$K_0 = \frac{b^*}{\delta_0} + h_1 \cos \sqrt{\delta_0} z + h_2 \sin \sqrt{\delta_0} z, \tag{8.30}$$

where h_1 and h_2 are integral constants. To obtain bounded solution for K_1 in (8.28), δ_0 must be zero. This will lead to an unbounded solution for K_0. Hence, if the perturbation method is applicable, we find that *for small ε, the small shearing on an inclined surface is unstable for $\hat{t} \ll \tau$.* Physically, this unstability is attributed to the coupled motion between shearing and torsion. When $\gamma \neq 0$, due to the gravitational effect, the energy stored in finite torsion is easily transported to shear motion. However, we should point out that all the conclusions in this section are valid only for $\hat{t} \ll \tau$ and are based on the perturbation method. We will address the accuracy of this approach later by numerical examples. For the moment, we shall explore the stability property of small shearing for the entire time region and then address the validity of the assumption of $\hat{t} \ll \tau$ used in this section.

8.2. Small shearing in the entire time region

The approach used by Beatty and Bhattacharyya [4] in the study of the Poynting oscillations of a rigid disk supported by a neo-Hookean rubber is adopted here to study the stability property of small shearing for the entire time region. We shall begin with the governing equation (8.15) as

$$K'' + [a + q \cos 2\phi]K = \hat{g} \tag{8.31}$$

and introduce the transformation (8.9)

$$\hat{t} = \frac{1}{\nu} \int_0^{\phi} \frac{d\psi}{\sqrt{1 - k^2 \sin^2 \psi}}. \tag{8.32}$$

Hence, we find

$$\frac{\mathrm{d}\phi}{\mathrm{d}\hat{t}} = v\sqrt{1-k^2\sin^2\phi}, \tag{8.33}$$

$$\frac{\mathrm{d}^2\phi}{\mathrm{d}\hat{t}^2} = -v^2k^2\sin\phi\cos\phi. \tag{8.34}$$

Since

$$\frac{\mathrm{d}K}{\mathrm{d}\hat{t}} = \frac{\mathrm{d}K}{\mathrm{d}\phi}\frac{\mathrm{d}\phi}{\mathrm{d}\hat{t}}, \quad \frac{\mathrm{d}^2K}{\mathrm{d}\hat{t}^2} = \frac{\mathrm{d}^2K}{\mathrm{d}\phi^2}\left(\frac{\mathrm{d}\phi}{\mathrm{d}\hat{t}}\right)^2 + \frac{\mathrm{d}K}{\mathrm{d}\phi}\frac{\mathrm{d}^2\phi}{\mathrm{d}\hat{t}^2}, \tag{8.35}$$

the transformation (8.32) reduces equation (8.31) to

$$\frac{\mathrm{d}^2K}{\mathrm{d}\phi^2} + 2P(\phi)\frac{\mathrm{d}K}{\mathrm{d}\phi} + R(\phi)K = g_1(\phi), \tag{8.36}$$

where

$$P(\phi) = -\frac{1}{2}\frac{k^2\sin\phi\cos\phi}{1-k^2\sin^2\phi}, \tag{8.37}$$

$$R(\phi) = \frac{v_K^2(1-k_K^2\sin^2\phi)}{v^2(1-k^2\sin^2\phi)}, \tag{8.38}$$

$$g_1(\phi) = \frac{\hat{g}}{v^2(1-k^2\sin^2\phi)}. \tag{8.39}$$

Parameters v and k are given by (8.10), and two new parameters, v_K and k_K, are defined through (8.16) and are given by

$$v_K = \sqrt{\omega_K^2 + \mu_K H_0^2} = \sqrt{\frac{2}{\lambda_s} + \frac{2\beta R_0^2 H_0^2}{\lambda_s^2}}, \tag{8.40}_1$$

$$k_K = \sqrt{\frac{\mu_K H_0^2}{\omega_K^2 + \mu_K H_0^2}} = \sqrt{\frac{1}{1+\dfrac{\lambda_s}{\beta R_0^2 H_0^2}}}. \tag{8.40}_2$$

Using the substitution

$$K = y\exp\left(-\int^{\phi} P(\psi)\,\mathrm{d}\psi\right) \tag{8.41}$$

in (8.36), we obtain the equation of motion in the form of

$$\frac{\mathrm{d}^2 y}{\mathrm{d}\phi^2} + D(\phi) y = g_2(\phi), \tag{8.42}$$

where

$$D(\phi) = R(\phi) - P^2(\phi) - \frac{\mathrm{d}P(\phi)}{\mathrm{d}\phi}, \tag{8.43}$$

$$g_2(\phi) = g_1(\phi) \exp\left(\int^{\phi} P(\psi)\, \mathrm{d}\psi \right). \tag{8.44}$$

Using (8.37) in (8.41) yields

$$K = \frac{y}{(1 - k^2 \sin^2 \phi)^{1/4}}. \tag{8.45}$$

This is the specific form of the transformation we used in reducing (8.36) to (8.42). Using (8.37), (8.38), and (8.39) in (8.43) and (8.44), we find

$$D(\phi) = \frac{v_K^2 (1 - k_K^2 \sin^2 \phi)}{v^2 (1 - k^2 \sin^2 \phi)} - \frac{k^2 (1 + \sin^2 \phi)}{4(1 - k^2 \sin^2 \phi)} + \frac{3k^2 \cos^2 \phi}{4(1 - k^2 \sin^2 \phi)^2}, \tag{8.46}$$

$$g_2(\phi) = \frac{\hat{g}}{v^2 (1 - k^2 \sin^2 \phi)^{3/4}}. \tag{8.47}$$

Hence, $D(\phi)$ and $g_2(\phi)$ are even periodic functions of ϕ of period π. For the motion of the disk on the horizonal surface with $\gamma = 0$, we find from $(7.14)_2$ and (5.3) that $g_2(\phi) = 0$. In this case, (8.42) is called the Hill's equation. In the following, we shall proceed in two directions: (1) to study the stability of the horizontal motion; and (2) to study the stability of motion of the disk on an inclined surface.

8.2.1. Motions on a horizontal surface

In this case, the equation of motion (8.42) reduces to

$$\frac{\mathrm{d}^2 y}{\mathrm{d}\phi^2} + D(\phi) y = 0. \tag{8.48}$$

This equation is in the same form as equation (7.11) in [4]. Using the Floquet's theory outlined in [9] and a stability criterion developed by Bhattacharyya [10], Beatty and Bhattacharyya [4] studied the stability property of the Poynting oscillations of a rigid disk supported by a neo-Hookean rubber shaft. In this section, we shall adopt the same approach and techniques used in [4] to discuss the stability property of Hill's equation (8.48) with $D(\phi)$ given by (8.46).

According to Beatty and Bhattacharyya [4], we shall expand the even periodic function $D(\phi)$ in (8.48) into Fourier series over $[0, \pi]$:

$$D(\phi) = \sum_{m=-\infty}^{\infty} b_m \, e^{2mi\phi}, \tag{8.49}$$

where $b_m = b_{-m}$ are constants and $i = \sqrt{-1}$. If we write (8.49) in terms of the cosine function, we have

$$D(\phi) = b_0 + 2b_1 \cos 2\phi + 2b_2 \cos 4\phi + 2b_3 \cos 6\phi + \cdots. \tag{8.50}$$

Hence, the coefficients b_m may be obtained through

$$b_m = \frac{1}{\pi} \int_0^{\pi} D(\phi) \cos 2m\phi \, d\phi, \quad m = 0, 1, 2, \ldots. \tag{8.51}$$

By the Floquet's theory we may write the solution to (8.48) in the form

$$y = e^{\zeta\phi} \sum_{m=-\infty}^{\infty} a_m \, e^{2mi\phi}, \tag{8.52}$$

where a_m are unknown constants. The stability of solution (8.52) hence is entirely determined by the stability index ζ. By substituting (8.49) and (8.52) into (8.48), we obtain the following infinite set of linear algebraic equations for the constants a_m:

$$(\zeta + 2im)^2 a_m + \sum_{p=-\infty}^{\infty} b_p a_{m-p} = 0, \quad (m = \ldots, -1, 0, 1, \ldots). \tag{8.53}$$

To obtain a nontrivial solution of (8.53), the determinant of the infinite coefficient matrix of a_m must vanish. We apply the same technique used by Beatty and Bhattacharyya in [4] to divide the m-th row by $b_0 - 4m^2$

($b_0 \neq 4m^2$) in securing its convergence and obtain the Hill's infinite determinant:

$$\Delta(i\zeta) = \begin{vmatrix} \cdots & \cdots & \cdots & \cdots & \cdots \\ \cdots & \dfrac{(i\zeta+2)^2 - b_0}{2^2 - b_0} & -\dfrac{b_1}{2^2 - b_0} & -\dfrac{b_2}{2^2 - b_0} & \cdots \\ \cdots & -\dfrac{b_1}{0^2 - b_0} & \dfrac{(i\zeta)^2 - b_0}{0^2 - b_0} & -\dfrac{b_1}{0^2 - b_0} & \cdots \\ \cdots & -\dfrac{b_2}{2^2 - b_0} & -\dfrac{b_1}{2^2 - b_0} & \dfrac{(i\zeta-2)^2 - b_0}{2^2 - b_0} & \cdots \\ \cdots & \cdots & \cdots & \cdots & \cdots \end{vmatrix} = 0. \quad (8.54)$$

On the other hand, it is shown in [9] that

$$\Delta(i\zeta) = \Delta(0) - \sin^2(i\pi\zeta/2)\cos^2(\pi\sqrt{b_0}/2), \quad (8.55)$$

where $\Delta(0) = \Delta(i\zeta)|_{\zeta=0}$. Hence, we obtain from (8.54) and (8.55)

$$\sin(i\pi\zeta/2) = \pm\sqrt{\Delta(0)}\sin(\pi\sqrt{b_0}/2). \quad (8.56)$$

At this point, we may recall a stability criterion developed by Bhattacharyya [10]: *If* $\Delta(0)$ *and* b_0 *have opposite sign, then* ζ *is a nonzero real-valued quantity; and hence, the solution* (8.52) *of Hill's equation* (8.48) *is unstable. If* $\Delta(0)$ *and* b_0 *are real-valued and have the same sign, the solution of* (8.48) *is stable if and only if*

$$|\sin(i\pi\zeta/2)| = |\sqrt{\Delta(0)}\sin(\pi\sqrt{b_0}/2)| \leqslant 1. \quad (8.57)$$

Since K and y are related through (8.45), the stability of small shearing is then entirely determined by the stability of y. Hence, in the following, we shall look at the stability property of y under different values of the physical parameters. This, of course, has to be accomplished through the numerical method.

We shall start with the Fourier series of $D(\phi)$ given by (8.49) or (8.50). The even periodic function $D(\phi)$ of period π given by (8.46) contains parameters k^2, k_K^2, and v_K^2/v^2. By (8.40) and (8.10) we find

$$k^2 = \frac{1}{2 + \dfrac{3\lambda_s}{\beta R_0^2 H_0^2}}, \quad (8.58)$$

$$k_K^2 = \frac{1}{1 + \dfrac{\lambda_s}{\beta R_0^2 H_0^2}}, \tag{8.59}$$

$$\frac{v_K^2}{v^2} = \frac{1}{d^2} \frac{6\lambda_s^2 + 6\lambda_s \beta R_0^2 H_0^2}{3\lambda_s + 2\beta R_0^2 H_0^2}. \tag{8.60}$$

Hence, $D(\phi)$ is a function of the following parameters: λ_s, the static longitudinal stretch; β, the material ratio defined by $(7.14)_1$; d, the gyration ratio defined by (6.7); R_0 the radius of the rubber cylinder; H_0, the initial torsion of the cylinder. It has been found through numerical calculation that the product $R_0 H_0$ provides more physically meaningful results than that of the case where R_0 and H_0 are treated as separate parameters for the stability property of y. Hence, we shall conduct our numerical computation for the wide range of values of four physical parameters: λ_s, β, d, and $R_0 H_0$. Among these four parameters, λ_s, β, d, and R_0 are positive. It is possible to have negative initial torsion H_0. However, since $H(t)$ is periodic and any negative initial torsion is equivalent to its corresponding positive H_0, we may assume without loss of generality that H_0 is positive.

We shall now decide the possible values these four parameters may assume. For static longitudinal stretch λ_s, the spring is pre-compressed if $0 < \lambda_s < 1$ and is pre-extended if $\lambda_s > 1$. When $\lambda_s = 1$, the rubber spring is in its natural state. Hence, we may choose $\lambda_s = 0.5$, 1, and 2. For the material ratio β we find from $(7.14)_1$ and (7.9) through (7.13) that the motion is linear when $\beta = 0$. Larger values of β correspond to stronger nonlinearity. Typically, we may choose $\beta = 0.05$, 0.5, and 1. For gyration ratio d defined by (6.7), we find that $d = \sqrt{2} R_0 / R_d$, where R_d is the radius of the disk. When the cylinder has the same radius as the disk, $d = \sqrt{2}$. Generally, $R_0 < R_d$. Hence, we may choose $d = 0.3$, 0.5, 1, and $\sqrt{2}$. Since $R_0 H_0$ is positive, we may give some estimate on the possible large values it may assume. For a large cylinder of radius of 0.2 meter and of length 1 meter under an initial stretch $\lambda_s = 0.2$, we find from (3.1) that an initial angle of twist of 2π (360°) corresponds to $R_0 H_0 = 6.28$. Hence, it is reasonable to assume that the possible value of parameter $R_0 H_0$ is in the range of (0, 10). According to this estimate, we conducted numerical calculations of the stability property of y for the following range of values of the four parameters:

$$\lambda_s \in [0.2, 4], \quad \beta \in [0.05, 2], \quad d \in [0.01, 10], \quad R_0 H_0 \in [0.01, 10]. \tag{8.61}$$

We see that the range we chose is much more than that likely to occur in a physical problem. By the stability theory briefed above, the following results have been observed from the numerical calculation:

1. The coefficients b_m in (8.51) for the Fourier series of $D(\phi)$ in (8.50) converges extremely fast for all values of (8.61). This implies that one may use the first few terms in (8.50) in approximating $D(\phi)$. This will greatly reduce the amount of work in calculating the Hill's infinite determinant (8.54).

2. For larger λ_s, smaller β, and smaller R_0H_0, the function $D(\phi)$ tends to become a positive constant independent of ϕ. The dominant term in (8.50) for this case is b_0 with $b_m \ll b_0$ for $m \geqslant 1$. By (8.58) and (8.59) we find that larger λ_s, smaller β and R_0H_0 correspond to smaller values of k and k_K. We indeed found under this situation that k and k_K are almost zero. Hence, we obtain from (8.46) that $D(\phi) \approx v_K^2/v^2$, a positive constant. In this case, by (8.48), (8.45), and (8.32) we find

$$K'' + v_K^2 K = 0. \tag{8.62}$$

Hence, the shearing motion is simple harmonic and hence stable. From $(8.40)_1$ we see that the frequency response v_K depends on the initial torsion H_0 due to the nonlinearity of the spring. When $q_1 = 0$, a case of linear motion, we find $\mu_K = 0$ and $v_K = \omega_K$, the frequency for linear spring which is independent of the initial condition H_0.

3. When λ_s gets smaller, β and R_0H_0 get larger, and the Fourier coefficient b_1 in (8.50) gets larger. However, we still find $b_m \ll b_0, b_1$ for $m \geqslant 2$. Hence, the dominant terms in (8.50) are b_0 and b_1. With these observations we may conclude that for all values of the four parameters given by (8.61), the dominant terms of the Fourier series for the function $D(\phi)$ are the first two terms in (8.50). We indeed found that the first two terms in (8.50) give a good approximation for $D(\phi)$ for $\phi \in [0, \pi]$.

If we just keep the first two terms in (8.50) as an approximation for $D(\phi)$, then

$$D(\phi) = b_0 + 2b_1 \cos 2\phi. \tag{8.63}$$

Hence, (8.48) becomes Mathieu's equation whose stability property has been studied extensively. At this point we realize that although the stability study in Section 8.1.1 needs the condition of $\hat{t} \ll \tau$, nevertheless, the conclusion is qualitatively correct for the entire time region since the shearing motion is indeed governed by an equation which is very close to Mathieu's equation.

After these preliminary computations, we are now ready to construct the stability map, a class of boundary curves in the parameter space separating the stable regions from the unstable ones, for small shearing motion. Although the Fourier series of function $D(\phi)$ is dominated by the first two terms, we choose the first nine terms in our numerical calculation following Beatty and Bhattacharyya's approach [4]. Hence, the Hill's infinite determinant $\Delta(0)$

is calculated by using nine central rows and columns in (8.54) for $\zeta = 0$. Then we use the stability criterion developed by Bhattacharyya [10] to construct the stability map. Following the steps outlined by Beatty and Bhattacharyya [4] and inspired by the stability map in [8], we choose $1/d$ and R_0H_0 as the coordinates for the stability map. Hence, for a given material ratio β and a given longitudinal static stretch λ_s, the stable region is obtained by finding the boundary curves in $1/d - R_0H_0$ space. The stability maps for $\beta = 0.5$ and $\lambda_s = 0.5, 1, 2$ are provided in Figs. 8.8–8.10 according to the stability criterion developed by Bhattacharyya [10, 4]. The shaded area represents the unstable region. From there we find:

1. The stability map for y, and hence for shearing K, resembles the stability map for Mathieu's equation in Fig. 4.1 of [8]. This can be explained from two aspects. First, the differential equation (8.48) is essentially a Mathieu's equation for the values of parameters given by (8.61). Second, we find from

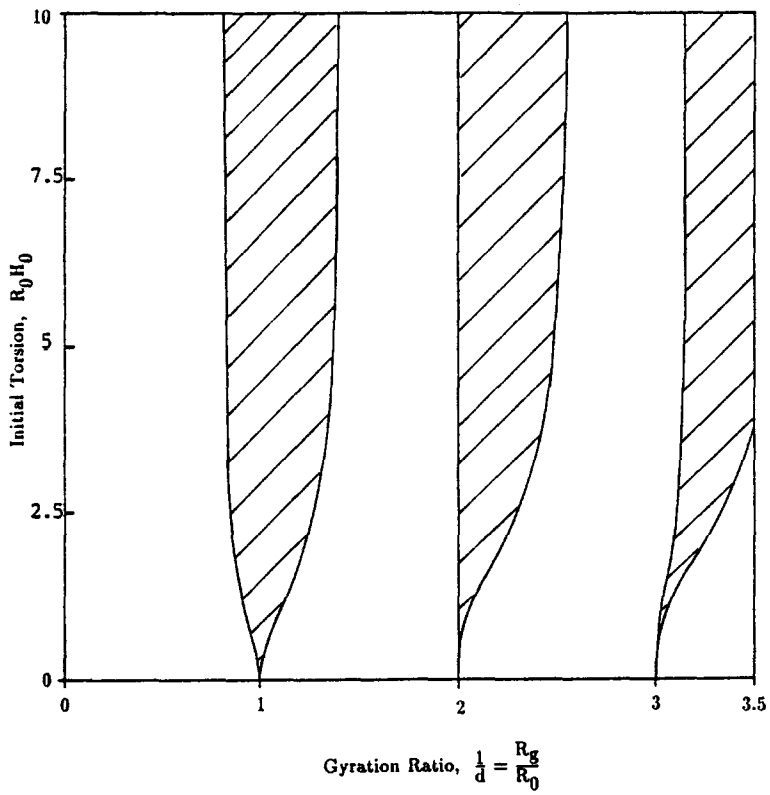

Fig. 8.8. Stability map of small shearing motion on the horizontal smooth surface coupled with finite amplitude torsional vibrations of a quadratic oscillator for $\beta = 0.5$ and $\lambda_s = 0.5$. The shaded areas are the unstable regions.

(8.23) that for fixed β and λ_s, δ is proportional to $1/d$ and ε is proportional to R_0H_0. Hence, the stability map of (8.48) on $1/d - R_0H_0$ space should have similar structures as that of Mathieu's equation (8.22) given by Fig. 4.1 in [8]. This resemblance also indicates that $1/d$ and R_0H_0 are good choices for the coordinates of the stability map.

2. Despite the resemblance, significant differences exist between the two maps. For Mathieu's equation, the stable regions are connected at the points $\delta = n^2/4$, $\varepsilon = 0$, n an integer. However, the stable regions for equation (8.48) are connected at the points $1/d = nC(\lambda_s)$, $R_0H_0 = 0$, where n is an integer and $C(\lambda_s)$ is a function of λ_s alone. $C(\lambda_s)$ has a value of 1, 0.707, 0.5 for $\lambda_s = 0.5$, 1, 2, respectively. Other values of C under different λ_s are shown in Fig. 8.11. We notice that $C(\lambda_s)$ is a decreasing function of λ_s. It approaches ∞ as $\lambda_s \to 0$. When $\lambda_s \to \infty$, it slowly approaches 0. We should point out from the numerical calculation that function $C(\lambda_s)$ shown in Fig. 8.11 is a universal one regardless of the material ratio β and hence is valid for all quadratic materials.

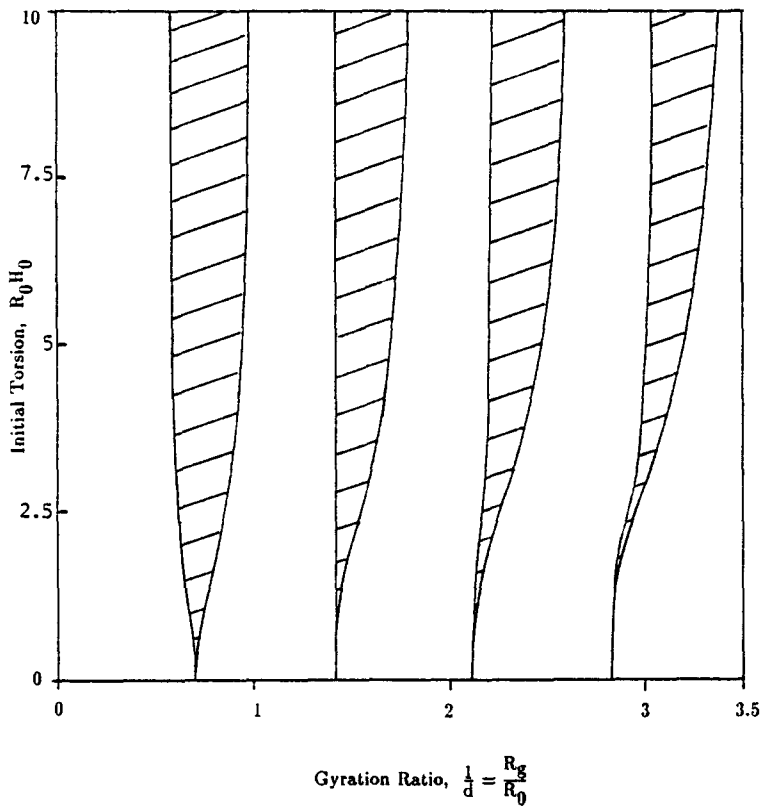

Fig. 8.9. Stability map of small shearing motion on the horizontal smooth surface coupled with finite amplitude torsional vibrations of a quadratic oscillator for $\beta = 0.5$ and $\lambda_s = 1.0$. The shaded areas are the unstable regions.

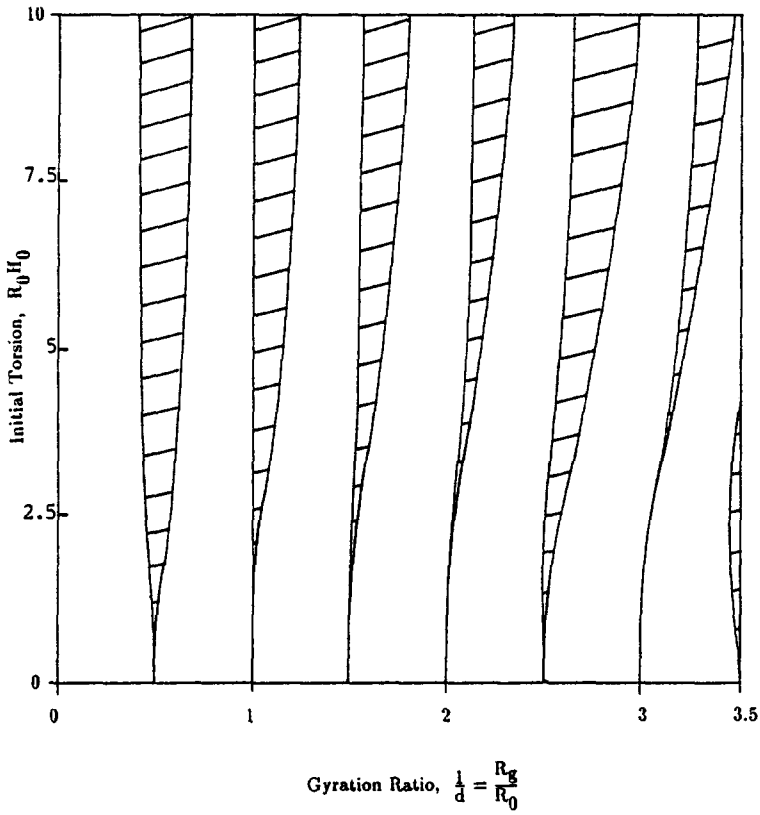

Fig. 8.10. Stability of small shearing motion on the horizontal smooth surface coupled with finite amplitude torsional vibrations of a quadratic oscillator for $\beta = 0.5$ and $\lambda_s = 2.0$. The shaded areas are the unstable regions.

To see the effect of the material ratio β, we construct the stability map shown in Fig. 8.12 for $\beta = 0.05$, 0.5, 1.0 and for $\lambda_s = 0.5$. We find that the unstable region gets bigger as β increases. This confirms our expectation since larger β means stronger nonlinearity. Although the boundary curves on the map vary as β changes, the connecting points of the stable regions do not change, a universal property discussed in the previous paragraph.

We are now ready to see some applications of the stability maps. The first numerical integration of equations (8.1) and (8.2) for the motions of a circular disk on a smooth horizontal surface is conducted for the case of $d = 1.0$ and $R_0H_0 = 2.5$. Other parameters are $\beta = 0.5$ and $\lambda_s = 0.5$. This point clearly falls into the unstable region on the stability map Fig. 8.8. The motions of the disk starts from $(H_0, H_0') = (5, 0)$ and $(K_0, K_0') = (0.5, 0)$. Figure 8.13 shows that while the finite torsional motion keeps its constant amplitude, the

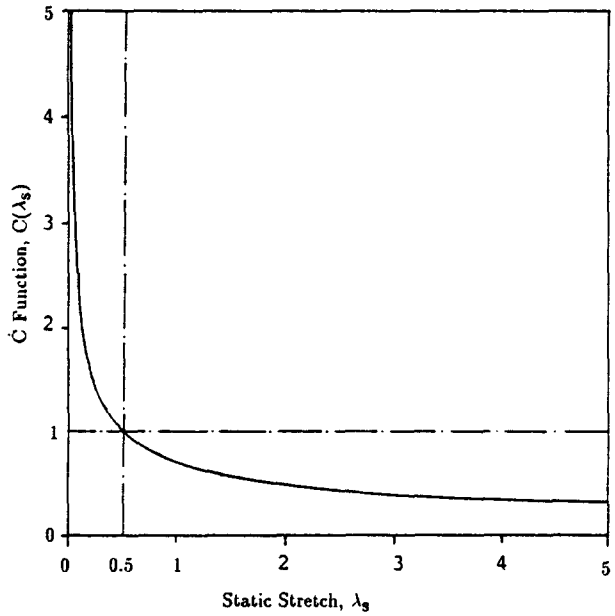

Fig. 8.11. Universal $C(\lambda_s)$ function of the stability property of small shearing motion on the horizontal smooth surface coupled with finite torsion of a quadratic oscillator.

small shearing motion builds up and diverges to infinity. The energy which drives the shearing motion to infinity, of course, comes from the torsional motion due to the coupling between the two equations. If we keep all the other physical parameters unchanged and switch d to $d = 2.0$, a point falling into the stable region on the stability map, the result is shown in Fig. 8.14. We see that both the torsional and shearing motions of the disk are constant periodic oscillations independent of each other. The stable motions do not interact with each other and no energy exchange is involved. These two examples support and demonstrate the validity of the stability maps developed from Bhattacharyya's Stability Criterion [10].

We also remember that equations (8.1) and (8.2) are approximations of the general governing equations (7.9) and (7.10) by assuming small shearing motion. In reality, the shearing motion cannot reach infinity, even when the physical parameters fall into an unstable region. Figure 8.15 shows the numerical integration of equations (7.9) and (7.10) for the same physical parameters used in Fig. 8.13. The small shearing motion is unstable, its amplitude builds up significantly compared with its initial position, reaches to a certain extent and then drops. In the meantime, the amplitude of torsional motion drops while $K(\hat{t})$ builds up and returns to its original magnitude as $K(\hat{t})$ drops. This clearly shows the energy exchange between two different phases of

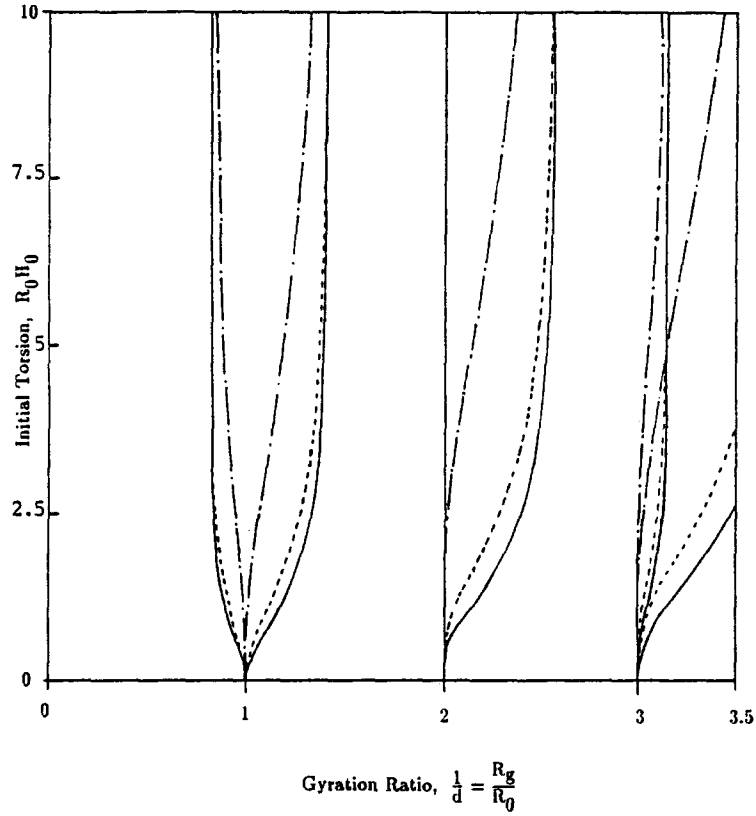

Fig. 8.12. Stability map of small shearing motion on the horizontal smooth surface coupled with finite torsion of a quadratic oscillator for $\lambda_s = 0.5$ and for various values of β. ——: $\beta = 0.05$, – – –: $\beta = 0.5$, — · — · —: $\beta = 1.0$.

the motions of the disk. The effect of coupling and the beating phenomenon of the motion is apparent in Fig. 8.15.

On the other hand, the exact solution of (7.9) and (7.10) for the stable oscillations shows no difference from that obtained from (8.1) and (8.2), which is shown in Fig. 8.14.

8.2.2. Motions on an inclined surface

In this case, we shall look at equation (8.31) whose coefficients a and q are given by (8.16) and (7.12):

$$q \equiv \tfrac{1}{2}\mu_K H_0^2 = \frac{\beta R_0^2 H_0^2}{\lambda_s^2}, \tag{8.64}$$

$$a \equiv \omega_K^2 + \tfrac{1}{2}\mu_K H_0^2 = \frac{2}{\lambda_s} + \frac{\beta R_0^2 H_0^2}{\lambda_s^2} = \frac{2}{\lambda_s} + q. \tag{8.65}$$

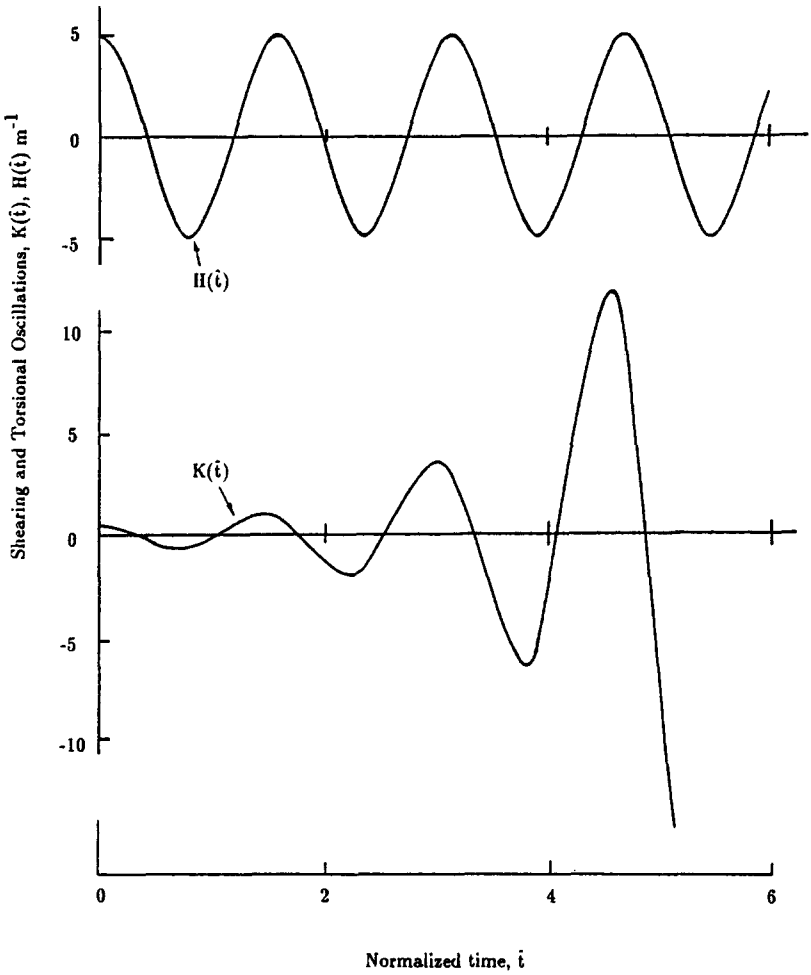

Fig. 8.13. Finite torsion and small shearing motions of a quadratic oscillator on smooth horizontal surface with $\beta = 0.5$, $\lambda_s = 0.5$, $d = 1$, $R_0 H_0 = 2.5$. This point falls into unstable region on the stability map in Fig. 8.8.

Hence, both a and q are functions of the material constant β. If β is small, a case of weak nonlinearity, q is also small. Hence, we may again use the perturbation method outlined in §8.1.2 to explore the stability property of the motion. The conclusion is apparent and the motion on the inclined surface in all cases is unstable. In the meantime, we also notice that the only difference between the motion on the horizontal suface and that on the inclined surface is the constant gravitational force in the shearing equation. One may expect that the conclusions about these two situations should be close to each other,

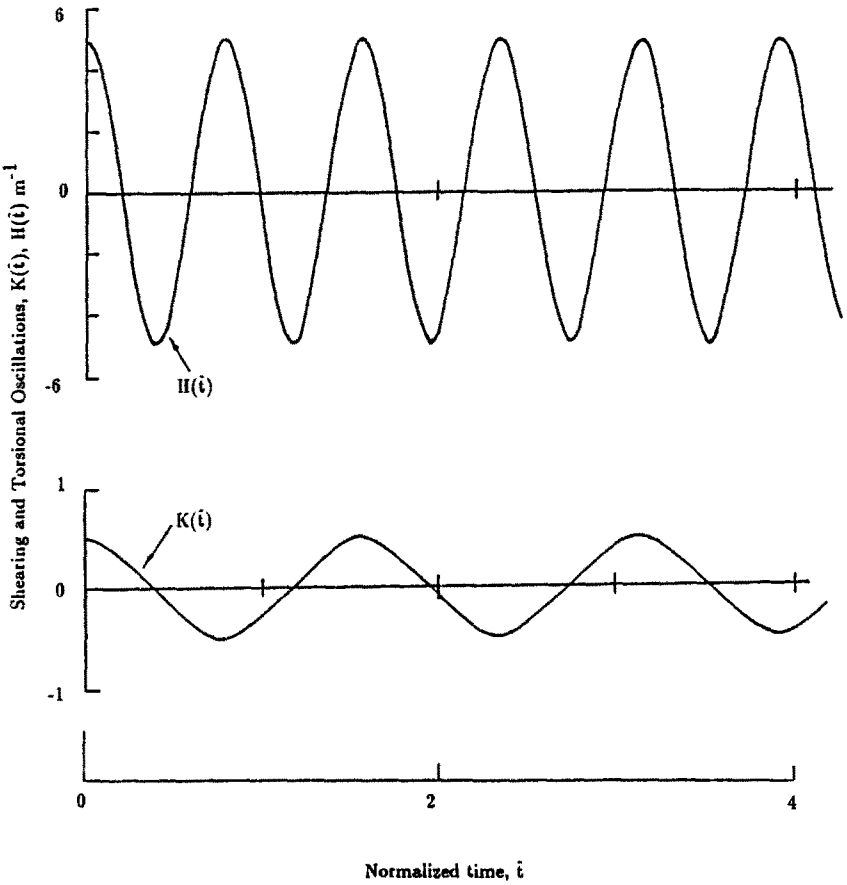

Fig. 8.14. Finite torsion and small shearing motions of a quadratic oscillator on smooth horizontal surface with $\beta = 0.5$, $\lambda_s = 0.5$, $d = 2$, $R_0 H_0 = 2.5$. This point falls into a stable region on the stability map in Fig. 8.8.

although the constant forcing term sometimes may cause significant complexity. With this in mind, we conducted numerical integrations of equations (8.1) and (8.2) for several values of the parameters. Figure 8.16 is the solution for the case of $\beta = 0.5$, $\lambda_s = 0.5$, $d = 1$, $R_0 H_0 = 2.5$. This point falls into the unstable region on the stability map in Fig. 8.8 for horizontal motion. The equilibrium position of K_s can be easily obtained from (8.1) which gives $\omega_K^2 K_s = \hat{g}$. The numerical integration is conducted for $K_s = 0.6$ with initial data of $(H_0, H_0') = (5, 0)$ and $K_0, K_0') = (1, 0)$. The small shearing motion diverges. The exact solution to (7.9) and (7.10) in this case is shown in Fig. 8.17 where the coupling and the beating are apparent. This example shows indeed the motion on the inclined surface is unstable.

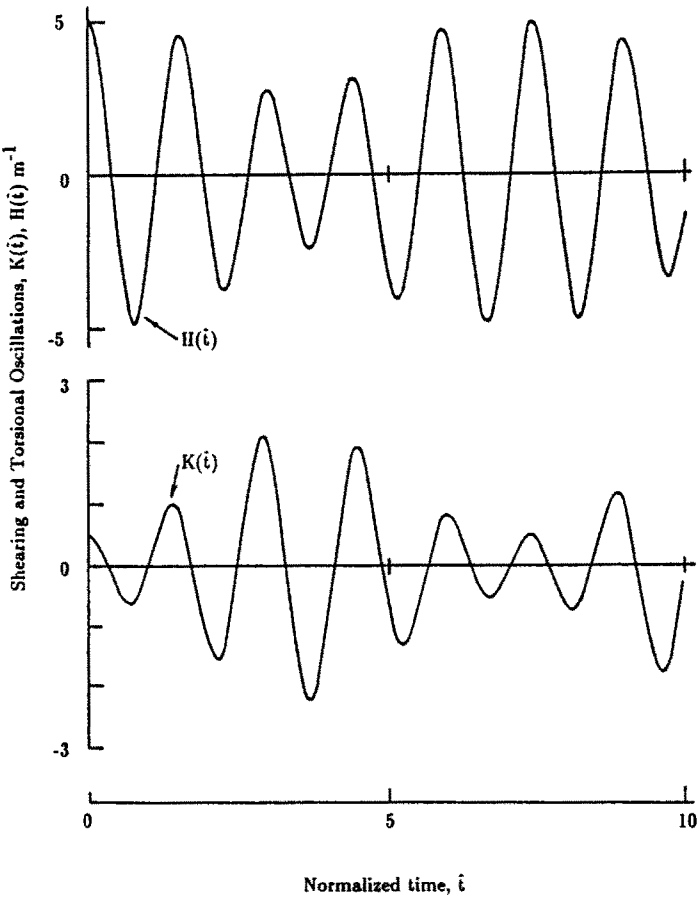

Fig. 8.15. Exact solutions of torsion and shearing motions computed from (7.9) and (7.10) for the unstable quadratic oscillator on the smooth horizontal surface with $\beta = 0.5$, $\lambda_s = 0.5$, $d = 2$, $R_0 H_0 = 2.5$. The energy exchange is apparent.

If we keep all the physical parameters and only change d to $d = 0.35$, a point falling into the stable region on the stability map in Fig. 8.8 for horizontal motion, we obtain the numerical solution of (8.1) and (8.2) shown in Fig. 8.18. Though the perturbation method predicted a divergent solution, the amplitude of oscillatory $K(\hat{t})$ does not go to infinity. We do see in Fig. 8.18 some build up on the amplitude of the shearing oscillation. However, the motion is essentially under control and exhibits beating phenomenon. The corresponding exact solutions of (7.9) and (7.10) in this case do not show significant difference. This example shows that the perturbation method does not necessarily provide valid answers to the stability problems in all situations.

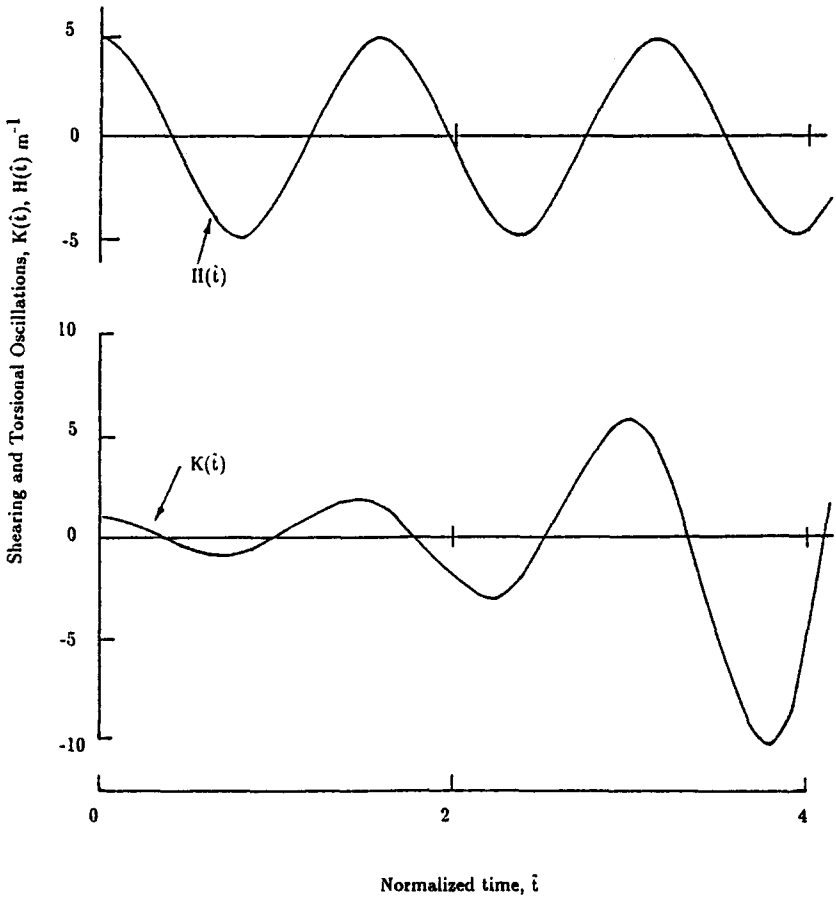

Fig. 8.16. Finite torsion and small shearing motions of a quadratic oscillator on the inclined surface with $\beta = 0.5$, $\lambda_s = 0.5$, $d = 1$, $R_0 H_0 = 2.5$, and $K_s = 0.6$. This point falls into an unstable region on the stability map in Fig. 8.8 for horizontal motion.

9. Stability of small torsion superimposed on finite shearing

For small torsion superimposed on finite shearing, the governing equations for the disk may be obtained by dropping the nonlinear terms in H in (7.9) and (7.10). Hence, we find for K and H

$$K'' + \omega_K^2 K + \varepsilon_K K^3 = \hat{g}, \tag{9.1}$$

$$H'' + \omega_H^2 H + \mu_H H K^2 = 0. \tag{9.2}$$

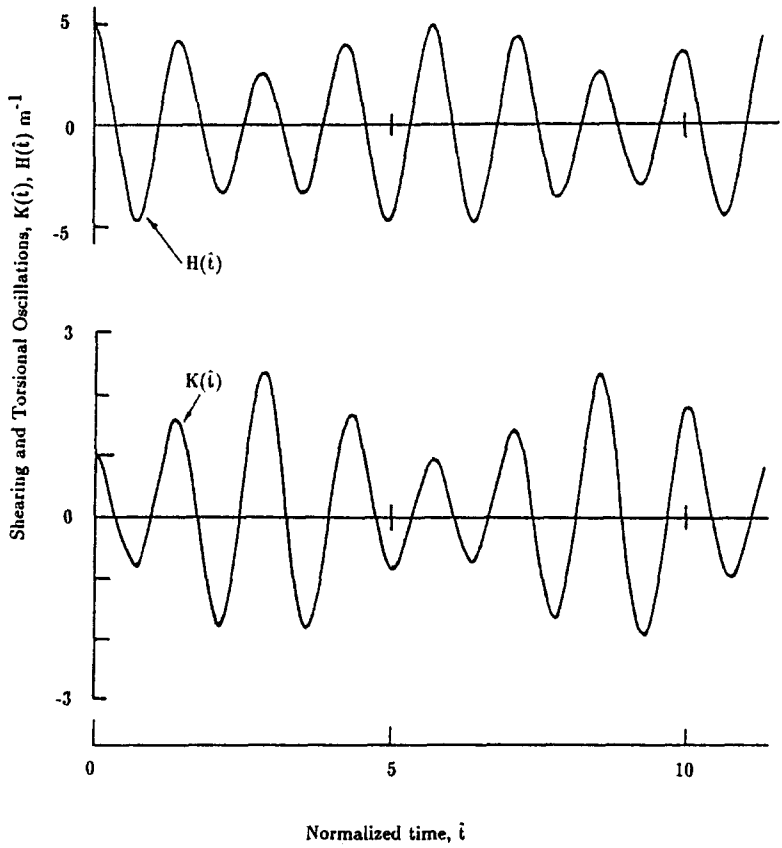

Fig. 8.17. Exact solutions of torsion and shearing motions computed from (7.9) and (7.10) for the unstable quadratic oscillator on the inclined surface with $K_s = 0.6$, $\beta = 0.5$, $\lambda_s = 0.5$, $d = 2$, $R_0 H_0 = 2.5$. Notice the energy exchange.

At this point, it is apparent that we shall pursue in two directions: (1) the motion on the horizontal surface; and (2) the motion on the inclined surface. Each case will feature different solutions for finite shearing K and the stability properties for small torsion H.

9.1. Motion of the disk on a smooth horizontal surface

In this case, equation (9.1) for the shearing reduces to

$$K'' + \omega_K^2 K + \varepsilon_K K^3 = 0. \tag{9.3}$$

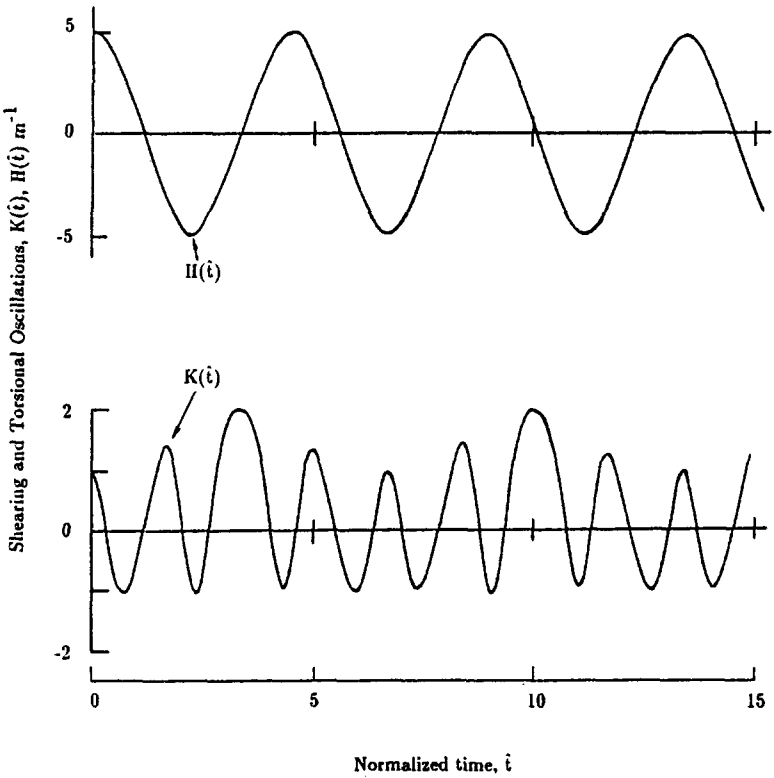

Fig. 8.18. Finite torsion and small shearing motions of a quadratic oscillator on the inclined surface with $\beta = 0.5$, $\lambda_s = 0.5$, $d = 0.35$, $R_0 H_0 = 2.5$, and $K_s = 0.6$. This point falls into a stable region on the stability map in Fig. 8.8 for horizontal motion.

This is again Duffing's equation whose closed form solution may be obtained in a similar way to that used in §8. By assuming the initial condition of $(K_0, 0)$ for K and using the transformation

$$K = K_0 \cos \psi, \tag{9.4}$$

the closed form solution of (9.3) is found to be

$$\hat{t} = \pm \frac{1}{v} \int_0^{\psi} \frac{\mathrm{d}\phi}{\sqrt{1 - \kappa^2 \sin^2 \phi}} = \pm \frac{1}{v} F(\psi, \kappa), \tag{9.5}$$

where

$$v = \sqrt{\omega_K^2 + \varepsilon_K K_0^2} = \sqrt{\frac{2}{\lambda_s}[1 + \beta K_0^2]},$$
$$\kappa = \sqrt{\frac{\varepsilon_K K_0^2}{2(\omega_K^2 + \varepsilon_K K_0^2)}} = \sqrt{\frac{1}{2 + \dfrac{2}{\beta K_0^2}}}, \tag{9.6}_1$$

and $F(\psi, \kappa)$ is again the elliptic integral of the first kind. The solution given by (9.5) for travel time $\hat{t}$ has a period of $\tau = (4/v)F(\pi/2, \kappa)$ in which $F(\pi/2, \kappa)$ is the complete elliptic integral of the first kind. It is clear that the period of the finite amplitude oscillations depends on the initial condition K_0. Similarly, we may find the period of the shearing motion in the form of

$$\tau = \frac{4}{v} F\left(\frac{\pi}{2}, \kappa\right) = \tau^* \frac{2F\left(\dfrac{\pi}{2}, \kappa\right)}{\pi\sqrt{1 + \dfrac{\varepsilon_K K_0^2}{\omega_K^2}}} = \tau^* \frac{2F\left(\dfrac{\pi}{2}, \kappa\right)}{\pi\sqrt{1 + \beta K_0^2}}, \tag{9.6}_2$$

where $\tau^* \equiv 2\pi/\omega_K$ is the period of the corresponding linear oscillator. We see that the normalized period τ/τ^* depends on β and K_0 only and is independent of the static stretch λ_s. The dependence of τ/τ^* on β and K_0 is demonstrated through Fig. 9.1 where τ/τ^* is plotted as a function of K_0 for various values of β. For all values of β, the normalized period of the motion is a decreasing function of the initial shearing K_0. When β increases, the nonlinearity of the material gets stronger, and τ/τ^* decreases. It is not difficult to see from $(9.6)_1$ and $(9.6)_2$ that when $\beta \to 0$, the material becomes linear, and $\tau/\tau^* \to 1$, as expected.

Solution (9.5) may also be written in terms of the Jacobian function

$$\psi = \pm \operatorname{sn} v\hat{t} = \pm \operatorname{sn}(v\hat{t}, \kappa). \tag{9.7}$$

Hence, the solution for finite shearing to equation (9.3) is given by

$$K = K_0 \cos[\operatorname{sn}(v\hat{t}, \kappa)]. \tag{9.8}$$

Thus, the shearing motion K is a periodic function with period $\tau = (4/v)F(\pi/2, \kappa)$. The phase diagrams of the motion are shown in Fig. 9.2 for various values of the initial shearing K_0. The finite shearing motion on the horizontal surface is symmetric about the equilibrium position, similar to that

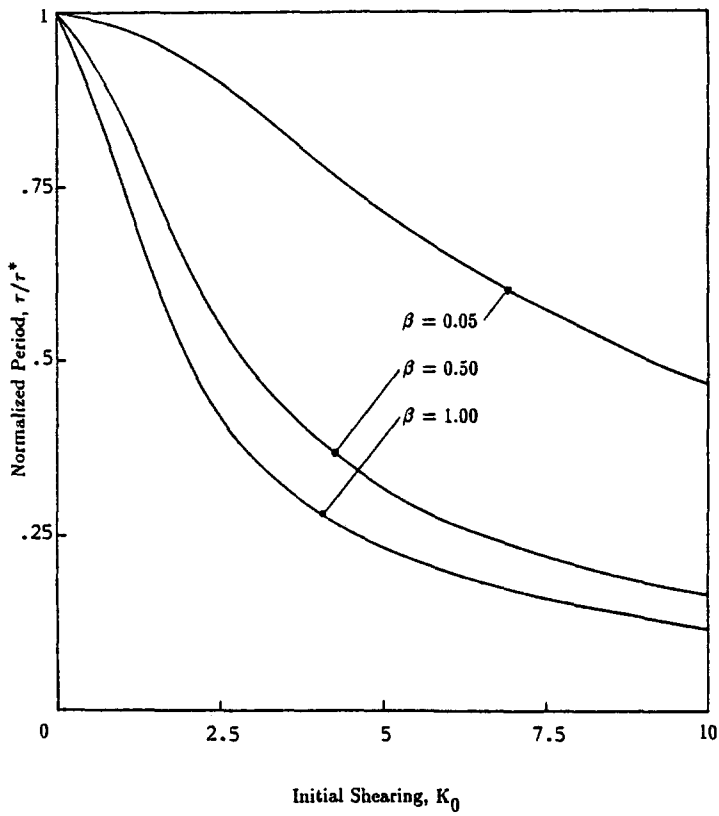

Fig. 9.1. Dimensionless period as a function of the initial shearing K_0 for finite amplitude shearing motions of a quadratic oscillator on a horizontal smooth surface for selected values of β.

of the torsional motion in Chapter 8. Figure 9.3 is the phase diagrams of the motion under various values of static stretch λ_s. As λ_s increases, the speed $H'(\hat{t})$ decreases and hence longer period. The phase diagrams of the motion for different values of β are shown in Fig. 9.4. When β increases, the speed $H'(\hat{t})$ increases and hence shorter period, an expected property since τ/τ^* is a decreasing function of β shown in Fig. 9.1. The finite shearing motion is independent of the gyration ratio d, a property can be seen from (7.12).

By using (9.8) in (9.2) we find the equation for small torsion to be

$$H'' + (a + q\cos 2\psi)H = 0, \tag{9.9}$$

where ψ is given by (9.7) and

$$a \equiv \omega_H^2 + \tfrac{1}{2}\mu_H K_0^2, \quad q \equiv \tfrac{1}{2}\mu_H K_0^2. \tag{9.10}$$

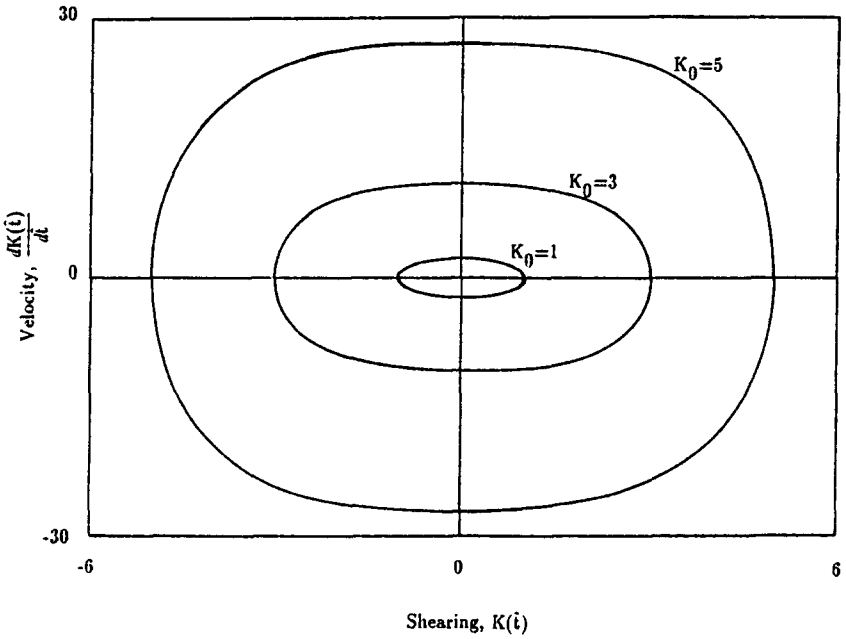

Fig. 9.2. Phase plane diagrams of the finite amplitude shearing motions of a quadratic oscillator on the horizontal smooth surface for $\beta = 0.5$, $\lambda_s = 0.5$, and for selected values of the initial data $(K_0, 0)$.

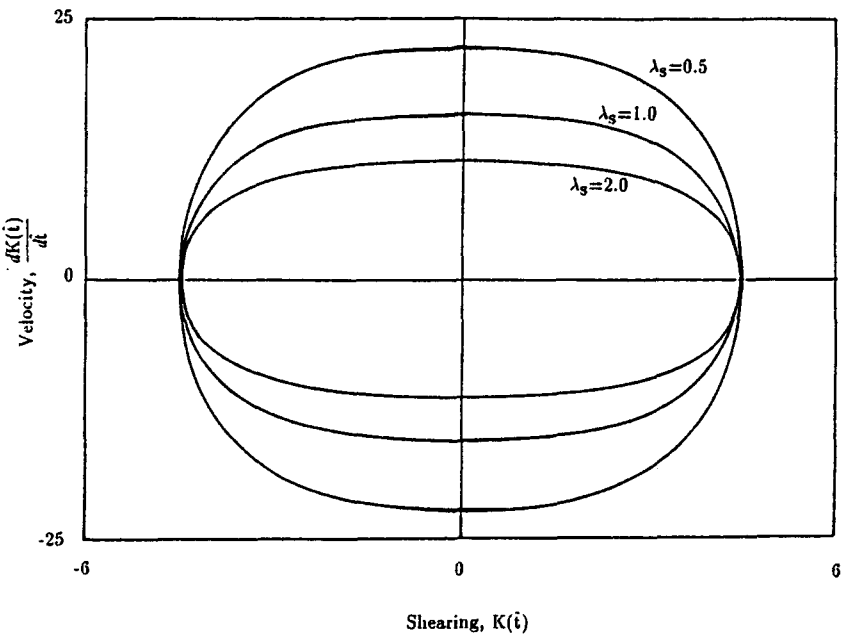

Fig. 9.3. Phase plane diagrams of the finite amplitude shearing motions of a quadratic oscillator on the horizontal smooth surface for $\beta = 0.5$, $K_0 = 4.5$ and for selected values of λ_s.

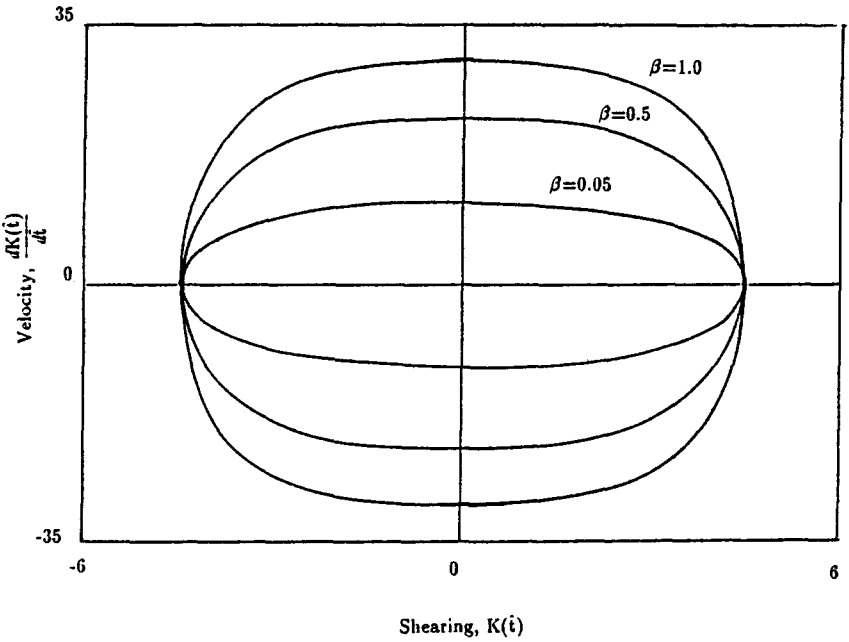

Fig. 9.4. Phase plane diagrams of the finite amplitude shearing motions of a quadratic oscillator on the horizontal smooth surface for $\lambda_s = 0.5$, $K_0 = 4.5$ and for selected values of β.

Equation (9.9) is identified as Hill's equation. Hence, the dynamical behavior of small torsion is similar to that of small shearing in Chapter 8. The same techniques may be used in exploring the stability properties of small H under different parameters and different initial conditions. First, we would like to look at the solution for $\hat{t} \ll \tau$.

9.1.1. Small torsion for $\hat{t} \ll \tau$

In following §8.1, by using the first term of the Taylor's series for the Jacobian elliptic function, equation (9.9) is reduced to

$$H'' + (a + q \cos 2v\hat{t})H = 0. \tag{9.11}$$

By using the transformation

$$z = 2v\hat{t} \tag{9.12}$$

in (9.11) we obtain

$$\frac{\mathrm{d}^2 H}{\mathrm{d}z^2} + (\delta + \varepsilon \cos z)H = 0, \tag{9.13}$$

where

$$\delta \equiv \frac{a}{4v^2}, \quad \varepsilon \equiv \frac{q}{4v^2}. \tag{9.14}$$

Here we again obtain the famous Mathieu's equation whose stability property is determined by locating the point (δ, ε) in the stability map. In order to find the dependence of the stability property of small H on the physical parameters, we use (9.14), (9.10), $(9.6)_1$, and (7.13) to find

$$\delta = \frac{d^2}{8\lambda_s}, \quad \varepsilon = \frac{d^2\beta K_0^2}{8\lambda_s(1+\beta K_0^2)} = \delta \frac{\beta K_0^2}{1+\beta K_0^2} = \frac{\delta}{1+\dfrac{1}{\beta K_0^2}}. \tag{9.15}$$

It is clear that small β which corresponds to weak nonlinearity produces small ε. According to the stability map in [8], the small torsion in this case is more likely stable. It is also true that the small initial shearing K_0 tends to stabilize the torsional motion. When $d \equiv R_0/R_g$ increases, ε becomes larger. Hence, for a fixed R_0 of the rubber cylinder, the larger inertia of the disk tends to stabilize the torsional motion. This conclusion matches our experience. We recall the discussion in §8.1.1 and remember that the conclusion of ε on d for small shearing is the opposite.

9.1.2. Small torsion for all $\hat{t}$

For the torsional motion in the entire time region, we may follow the approach outlined in §8.2 to introduce the transformation

$$\hat{t} = \frac{1}{v}\int_0^{\psi} \frac{\mathrm{d}\phi}{\sqrt{1-\kappa^2\sin^2\phi}} \tag{9.16}$$

in reducing equation (9.9) to

$$\frac{\mathrm{d}^2H}{\mathrm{d}\psi^2} + 2P(\psi)\frac{\mathrm{d}H}{\mathrm{d}\psi} + R(\psi)H = 0, \tag{9.17}$$

where

$$P(\psi) = -\frac{1}{2}\frac{\kappa^2\sin\psi\cos\psi}{1-\kappa^2\sin^2\psi}, \tag{9.18}$$

$$R(\psi) = \frac{v_H^2(1-\kappa_H^2\sin^2\psi)}{v^2(1-\kappa^2\sin^2\psi)}. \tag{9.19}$$

Parameters v and κ are given by $(9.6)_1$, and two new parameters, v_H and κ_H, are defined through (9.10) and are given by

$$v_H = \sqrt{\omega_H^2 + \mu_H K_0^2} = \frac{d}{\lambda_s}\sqrt{1 + 2\beta K_0^2}, \tag{9.20}$$

$$\kappa_H = \sqrt{\frac{\mu_H K_0^2}{\omega_H^2 + \mu_H K_0^2}} = \sqrt{\frac{1}{1 + \dfrac{1}{2\beta K_0^2}}}. \tag{9.21}$$

Using the substitution

$$H = y \exp\left(-\int^{\psi} P(\phi)\, \mathrm{d}\phi\right) \tag{9.22}$$

in (9.17), we obtain the equation of motion in the form

$$\frac{\mathrm{d}^2 y}{\mathrm{d}\psi^2} + D(\psi) y = 0, \tag{9.23}$$

where

$$D(\psi) = R(\psi) - P^2(\psi) - \frac{\mathrm{d}P(\psi)}{\mathrm{d}\psi}, \tag{9.24}$$

Again using (9.18) in (9.22) yields

$$H = \frac{y}{(1 - \kappa^2 \sin^2 \psi)^{1/4}}, \tag{9.25}$$

which is the specific form of the transformation we used in reducing (9.17) to (9.23). Using (9.18), and (9.19) in (9.24) we find

$$D(\psi) = \frac{v_H^2(1 - \kappa_H^2 \sin^2 \psi)}{v^2(1 - \kappa^2 \sin^2 \psi)} - \frac{\kappa^2(1 + \sin^2 \psi)}{4(1 - \kappa^2 \sin^2 \psi)} + \frac{3\kappa^2 \cos^2 \psi}{4(1 - \kappa^2 \sin^2 \psi)^2}. \tag{9.26}$$

We see that the small torsional motion coupled with the finite shear has exactly the same mathematical structure as that of small shearing coupled with finite torsion studied in §8.2. The only differences between these two

problems are the parameters κ, κ_H, v, and v_H. Through the previous relations, we find that

$$\kappa^2 = \frac{1}{2 + \dfrac{2}{\beta K_0^2}}, \tag{9.27}$$

$$\kappa_H^2 = \frac{1}{1 + \dfrac{1}{2\beta K_0^2}}, \tag{9.28}$$

$$\frac{v_H^2}{v^2} = d^2 \frac{1 + 2\beta K_0^2}{2\lambda_s(1 + \beta K_0^2)}. \tag{9.29}$$

Here we again follow Beatty and Bhattacharyya's approach [4] outlined in §8.2 to conduct the stability analysis through numerical calculation. Using the stability criterion developed by Bhattacharyya [10], we conducted numerical calculations for a wide range of parameters

$$\lambda_s \in [0.2, 2], \quad \beta \in [0.05, 1], \quad d \in [0.01, 10], \quad K_0 \in [0.01, 10]. \tag{9.30}$$

In constructing the stability maps, we found that the Fourier coefficients for the function $D(\psi)$ converge very fast. For all values of (9.30), only the first two terms are significant. This demonstrates that small torsional motion is governed by an equation similar to Mathieu's equation. Nevertheless, we use the first nine terms of the Fourier approximation for function $D(\psi)$ for the sake of consistency.

Based on this condition, the stability maps for $\beta = 0.5$ and for selected values of λ_s are obtained as shown in Figs. 9.5–9.7. The stability maps are constructed by indicating the unstable regions in the $d - K_0$ plane. It has been seen that the stable regions are disconnected from each other. When λ_s increases, the unstable regions expand and shift in the positive d direction. To see the effect of β, we plotted the unstable regions for $\beta = 0.05$, 0.5, 1.0 in Fig. 9.8. Although the unstable region shifts, larger β which corresponds to stronger nonlinearity does not produce significant larger unstable region.

We are now ready to show some numerical applications of the stability map established for small torsional motion coupled with finite shearing. Figure 9.9 shows the result of numerical integration of equations (9.2) and (9.3) for $\beta = 0.5$, $\lambda_s = 2.0$, $d = 2.0$, $K_0 = 5.0$, $R_0 = 0.5m$. This point falls into the unstable region on the stability map in Fig. 9.7. The numerical solution is obtained for the initial data $(K_0, K_0') = (5, 0)$ and $(H_0, H_0') = (0.5, 0)$. We see, as expected,

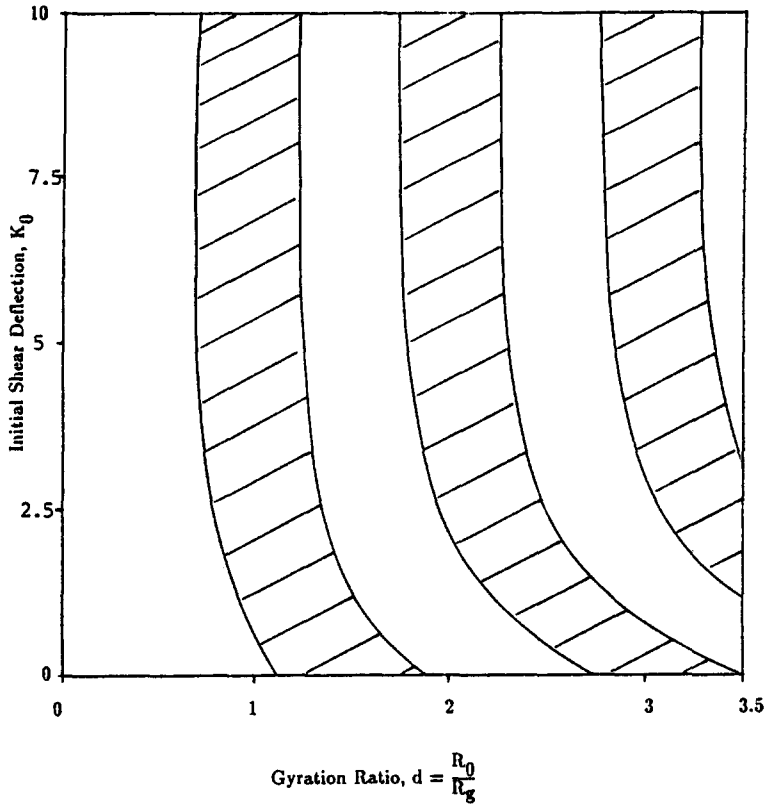

Fig. 9.5. Stability map of small torsional motion on the horizontal smooth surface coupled with finite shearing of a quadratic oscillator for $\beta = 0.5$ and $\lambda_s = 0.5$. The shaded areas are the unstable regions.

that the small torsional motion diverges to infinity while the finite shearing keeps its constant amplitude oscillations. The corresponding exact solution of equations (7.9) and (7.10) for the same physical parameters is shown in Fig. 9.10. Instead of seeing the divergent solution for $H(\hat{t})$, we find the nonlinear coupling and the energy exchange between two different parts of the motions as well as the beating phenomenon.

In keeping all the physical parameters used in Figs. 9.9 and 9.10 except switching d to $d = 1.0$, Fig. 9.11 shows the numerical solutions of (9.2) and (9.3) with (d, K_0) falling into the stable region on the stability map in Fig. 9.7. The small torsion and the finite shearing are independent of each other. The numerical integration of (7.9) and (9.10), of course, generates the same

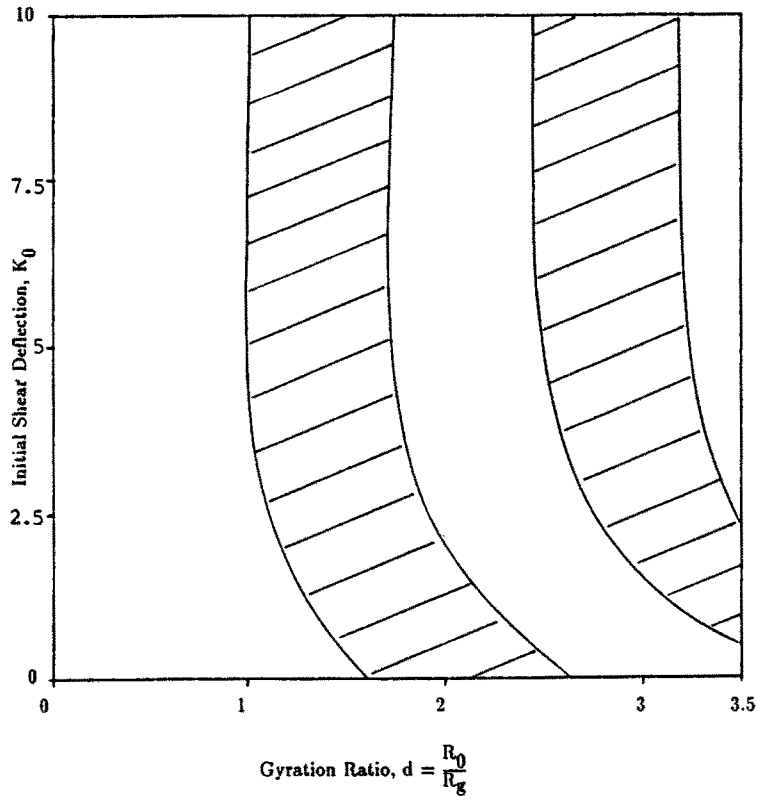

Fig. 9.6. Stability map of small torsional motion on the horizontal smooth surface coupled with finite shearing of a quadratic oscillator for $\beta = 0.5$ and $\lambda_s = 1.0$. The shaded areas are the unstable regions.

solution as shown in Fig. 9.11. These two examples demonstrate the validity of the stability maps and support again Bhattacharyya's Stability Criterion [10].

9.2. Motion of the disk on an inclined surface

For motions of the disk on an inclined surface with $\gamma \neq 0$, the governing equations are (9.1) and (9.2). The equilibrium position of the disk can be established from (9.1) and (9.2) as

$$\omega_K^2 K_s + \varepsilon_K K_s^3 = \hat{g}, \quad H_s = 0, \tag{9.31}$$

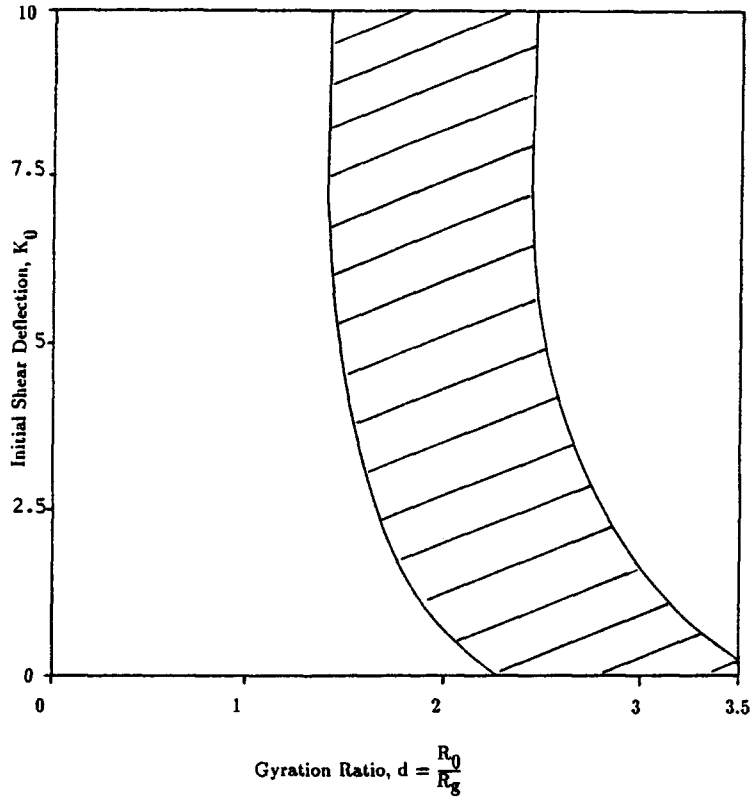

Fig. 9.7. Stability map of small torsional motion on the horizontal smooth surface coupled with finite shearing of a quadratic oscillator for $\beta = 0.5$ and $\lambda_s = 2.0$. The shaded area is the unstable region.

where K_s is the equilibrium static shear deflection. By multiplying K' on each side of (9.1) we obtain

$$K'K'' + \omega_K^2 K'K + \varepsilon_K K'K^3 - \hat{g}K' = 0. \tag{9.32}$$

For finite shearing motion, we assume in this case that the disk starts its motion from the most general initial position of (K_0, K_0'). Hence, equation (9.32) is integrated into

$$K' = \pm\sqrt{-\frac{\varepsilon_K}{2} f(K)}, \tag{9.33}$$

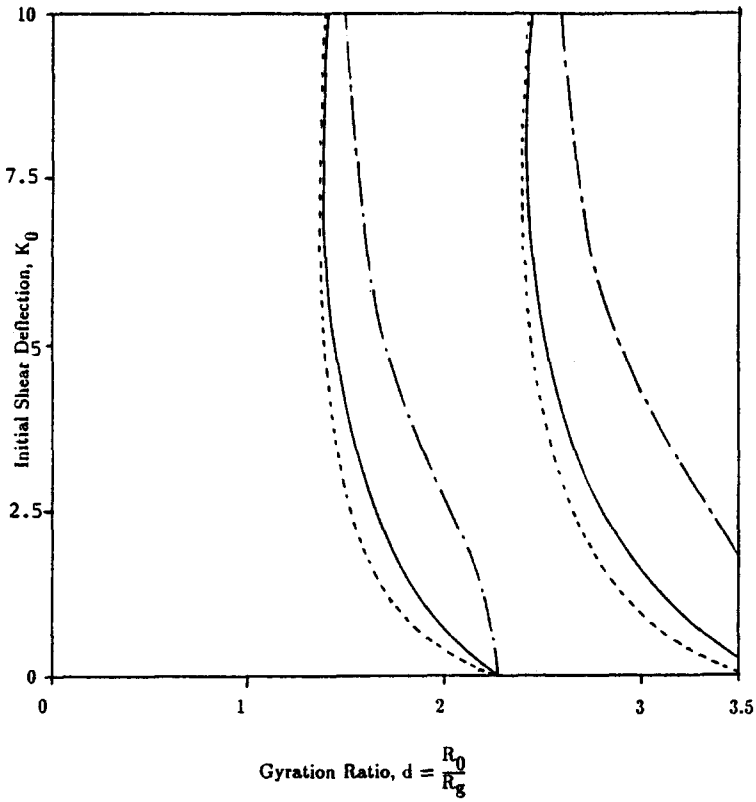

Fig. 9.8. Stability map of small torsional motion on the horizontal smooth surface coupled with finite shearing of a quadratic oscillator for $\lambda_s = 2.0$ and for various values of β. ---: $\beta = 0.05$, ——: $\beta = 0.5$, — - — - — - —: $\beta = 1.0$.

where

$$f(K) \equiv K^4 + \frac{2}{\beta} K^2 - \frac{4\hat{g}}{\varepsilon_K} K - \frac{4C}{\varepsilon_K}. \tag{9.34}$$

The material ratio

$$\beta = \frac{\varepsilon_K}{\omega_K^2} = \frac{q_1}{q_0} \tag{9.35}$$

was first introduced in $(7.14)_1$, and the energy constant C in (9.34) is given by

$$C = C(K_0, K_0') = \tfrac{1}{2}[K_0']^2 + \tfrac{1}{2}\omega_K^2 K_0^2 + \tfrac{1}{4}\varepsilon_K K_0^4 - \hat{g} K_0. \tag{9.36}$$

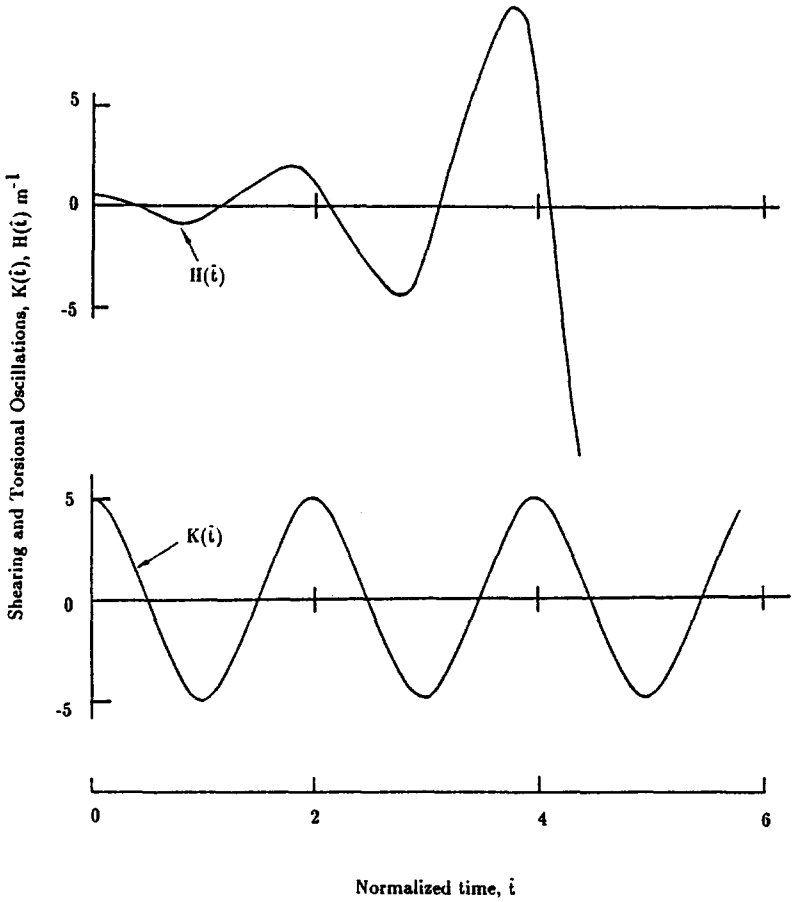

Fig. 9.9. Finite shearing and small torsional motions of a quadratic oscillator on a smooth horizontal surface with $\beta = 0.5$, $\lambda_s = 2$, $d = 2$, $K_0 = 5$, and $R_0 = 0.5$. This point falls into the unstable region on the stability map in Fig. 9.7.

Hence, the solution to (9.33) is given by

$$\hat{t} = \frac{\tau^*}{2\pi}\sqrt{\frac{2}{\beta}}\, I(K, \beta), \quad \tau^* \equiv \frac{2\pi}{\omega_K}, \tag{9.37}$$

wherein τ^* is the period of the corresponding linear oscillator and

$$I(K, \beta) \equiv \pm \int_{K_0}^{K} \frac{\mathrm{d}K}{\sqrt{-f(K)}}. \tag{9.38}$$

In view of (9.34) we realize that $I(K, \beta)$ is a general elliptic integral whose standard form depends on $f(K)$. This elliptic integral is similar to that of (3.6)

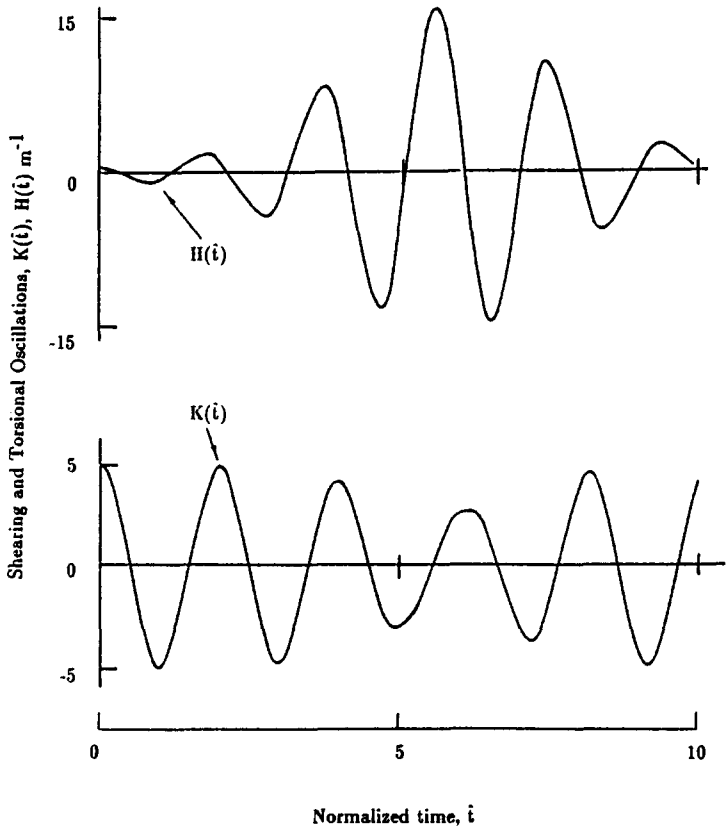

Fig. 9.10. Exact solutions of torsion and shearing motions computed from (7.9) and (7.10) for the unstable quadratic oscillator on a smooth horizontal surface with $\beta = 0.5$, $\lambda_s = 2$, $d = 2$, $K_0 = 5$, and $R_0 = 0.5$.

in [11] where the finite amplitude vibrations of a Mooney-Rivlin oscillator is studied. Hence, in the following, we shall follow Beatty and Chow [11] to reduce (9.38) to the standard form.

Apparently, $f(K)$ has two real roots, K_1, K_2, say. These two roots correspond to the extreme positions for shearing motion for which the speeds $K'(K_1)$ and $K'(K_2)$ vanish. It may be shown from this property or from the energy constant $C(K_1, 0) = C(K_2, 0)$ that the extreme shear deflections satisfy

$$(K_1 + K_2)\left(\frac{2}{\beta} + K_1^2 + K_2^2\right) = \frac{4\hat{g}}{\varepsilon_K}. \tag{9.39}$$

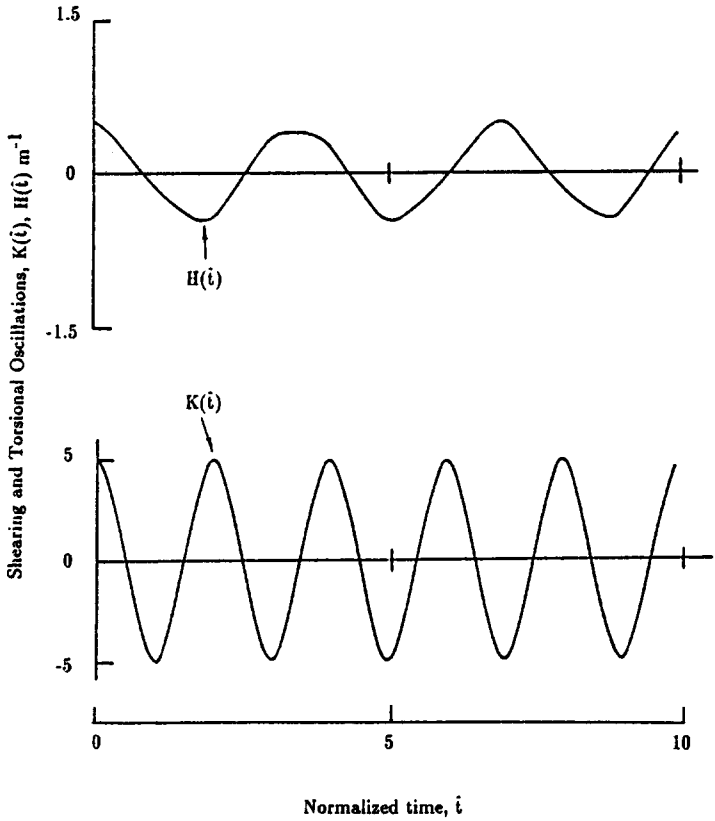

Fig. 9.11. Finite shearing and small torsional motions of a quadratic oscillator on a smooth horizontal surface with $\beta = 0.5$, $\lambda_s = 2$, $d = 1$, $K_0 = 5$, and $R_0 = 0.5$. This point falls into the stable region on the stability map in Fig. 9.7.

Hence, $f(K)$ may be rewritten as

$$f(K) = (K - K_1)(K - K_2)\left[K^2 + (K_1 + K_2)K + \frac{2}{\beta} - K_1K_2 + (K_1 + K_2)^2\right]. \tag{9.40}$$

It is also clear that the other two roots could be real, multiple, or complex depending on whether

$$S = (K_1 + K_2)^2 - 4\left[\frac{2}{\beta} - K_1K_2 + (K_1 + K_2)^2\right] \tag{9.41}$$

is greater, equal, or less than zero. We shall show that for our case, $S < 0$. To prove this, let us first assume that $S = 0$ to get

$$(K_1 + K_2)^2 = 4\left[\frac{2}{\beta} - K_1K_2 + (K_1 + K_2)^2\right]. \tag{9.42}$$

Bearing in mind the definition of β in (9.35), equations $(9.31)_1$ and (9.39) yield

$$(K_1 + K_2)\left(\frac{2}{\beta} + K_1^2 + K_2^2\right) = 4\left(\frac{K_s}{\beta} + K_s^3\right). \tag{9.43}$$

It may be shown that equations (9.42) and (9.43) yield

$$K_1 + K_2 = -2K_s, \tag{9.44}$$

$$K_1 K_2 = \frac{2}{\beta} + 3K_s^2, \tag{9.45}$$

and solutions

$$K_{1,2} = -K_s \pm \sqrt{-2K_s^2 - \frac{2}{\beta}}. \tag{9.46}$$

This shows that K_1 and K_2 are complex roots which contradicts our assumption. Hence, S cannot be zero. To prove that K_3 and K_4 are complex, we assume that K_3 and K_4 are real and $S > 0$. Then consider the following equations:

$$K_1 + K_2 = x, \quad K_1 K_2 = y. \tag{9.47}$$

It may be shown that in order to keep K_1 and K_2 real, we have to have

$$4y < x^2. \tag{9.48}$$

On the other hand, relation $S > 0$ yields

$$3x^2 < 4y - \frac{8}{\beta} < x^2 - \frac{8}{\beta} \tag{9.49}$$

which is

$$(K_1 + K_2)^2 < -\frac{4}{\beta}. \tag{9.50}$$

Since β is a positive constant, (9.50) cannot hold. Hence, K_3 and K_4 are two complex conjugate roots with $K_4 = \bar{K}_3$. Hence, (9.38) becomes

$$I(K, \beta) = \pm \int_{K_0}^{K} \frac{\mathrm{d}K}{\sqrt{(K - K_1)(K_2 - K)(K - K_3)(K - \bar{K}_3)}}. \tag{9.51}$$

Following Beatty and Chow [11], we introduce

$$N(K) \equiv \int_{K_1}^{K} \frac{\mathrm{d}K}{\sqrt{(K-K_1)(K_2-K)(K-K_3)(K-\bar{K}_3)}} \tag{9.52}$$

and the transformation

$$\xi(K) = \cos^{-1}\left[\frac{(K_2-K)Q_1-(K-K_1)Q_2}{(K_2-K)Q_1+(K-K_1)Q_2}\right], \tag{9.53}$$

to obtain

$$K = \frac{K_1Q_2 + K_2Q_1\tan^2(\xi/2)}{Q_2 + Q_1\tan^2(\xi/2)}. \tag{9.54}$$

In (9.53) and (9.54), the parameters Q_1 and Q_2 are given by

$$Q_l = Q(K_l) = \sqrt{K_l^2 + (K_1+K_2)K_l + \frac{2}{\beta} - K_1K_2 + (K_1+K_2)^2}, \quad l = 1, 2. \tag{9.55}$$

Substitution of (9.54) into (9.52) leads to

$$N(K) = \frac{F(\xi, k)}{\sqrt{Q_1Q_2}}, \tag{9.56}$$

where $F(\xi, k)$ is the elliptic integral of the first kind and the modulus k is given by

$$k = \sqrt{\frac{(K_1-K_2)^2 - (Q_1-Q_2)^2}{4Q_1Q_2}}. \tag{9.57}$$

Hence, the normalized time $\hat{t}$, which is the exact solution to (9.1), is found to be

$$\hat{t} = \pm\frac{\tau^*}{2\pi}\sqrt{\frac{2}{\beta}}[N(K) - N(K_0)] = \pm\frac{\tau^*}{2\pi}\sqrt{\frac{2}{\beta Q_1Q_2}}[F(\xi, k) - F(\xi_0, k)], \tag{9.58}$$

wherein $\xi = \xi(K)$ is given by (9.53) and $\xi_0 = \xi(K_0)$. It is easy to see from (9.53) that ξ varies between 0 and π when K goes from K_1 to K_2 in the half period $\tau/2$. Thus, the period of vibration τ is found to be

$$\tau = \tau^*\frac{2}{\pi}\sqrt{\frac{2}{\beta Q_1Q_2}}F\left(\frac{\pi}{2}, k\right). \tag{9.59}$$

By (9.55) and (9.57) we see that this period depends on the extreme shear deflections K_1, K_2, and material ratio β only. This dependence is demonstrated in Fig. 9.12 for the normalized period as a function of the extreme shear deflection K_2. In generating this and the next figure, the other extreme shear deflection K_1 is assumed to be 0. Hence, the shear motion is oscillating between 0 and K_2 with the oscillation center located at the middle of $[0, K_2]$. We see that the normalized period of the motion is similar to that of the motion on the horizontal surface. τ/τ^* is a decreasing function of the extreme shear deflection K_2. It is also a decreasing function of β. When β approaches 0, $\tau/\tau^* \to 1$, as we expected.

The closed form solution to finite amplitude oscillations of shearing on an inclined surface is given by (9.58). The phase plane diagrams of the motion for selected values of K_2 are shown in Fig. 9.13. Again, $K_1 = 0$ is assumed in generating the figures. It is apparent that the motion is asymmetric about the equilibrium static shear deflection K_s. The changes of the phase plane diagrams with respect to λ_s and β are shown in Figs. 9.14 and 9.15. It is shown

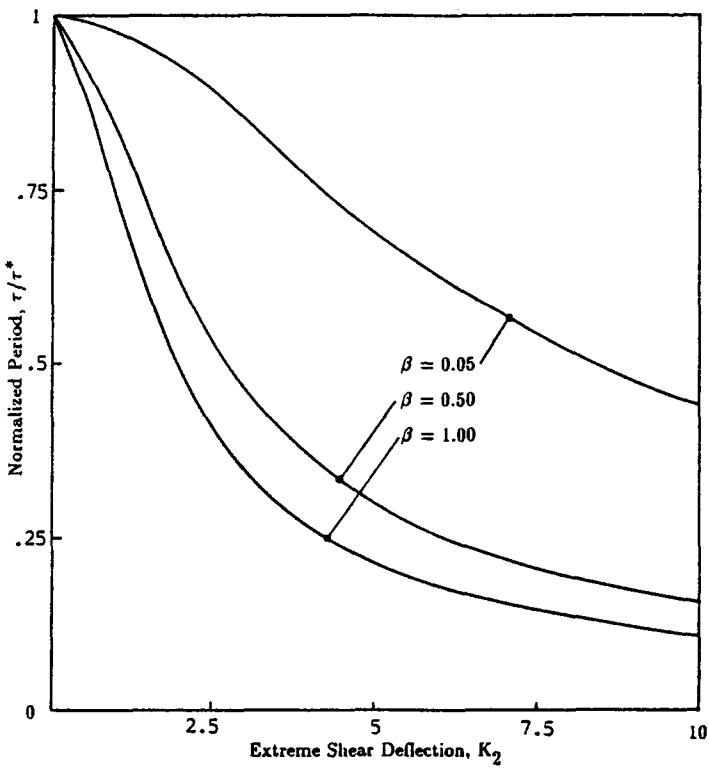

Fig. 9.12. Dimensionless period as a function of the extreme shearing K_2 for finite amplitude shearing motions of a quadratic oscillator on an inclined surface for selected values of β. The other extreme shear deflection K_1 is assumed to be 0.

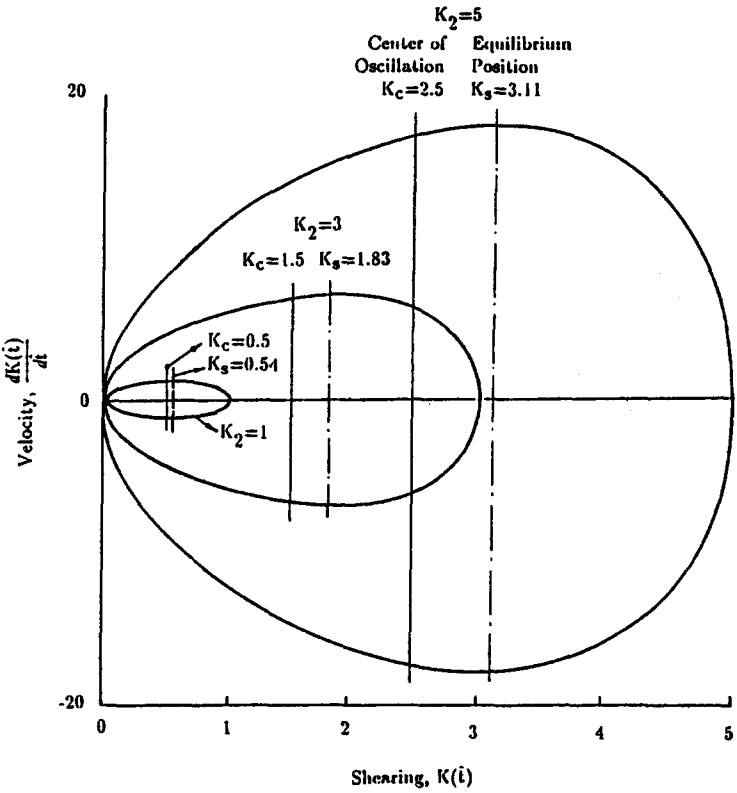

Fig. 9.13. Phase plane diagrams of the finite amplitude shearing motions of a quadratic oscillator on an inclined surface for $\beta = 0.5$, $\lambda_s = 0.5$, and for selected values of the extreme shear deflection K_2. The other extreme shear deflection K_1 is assumed to be 0.

that the patterns of the variation of the phase plane diagrams are similar to that of motions on the horizontal surface except in this case the oscillation is asymmetric about the equilibrium position K_s.

We are now ready to see some special cases. Since equation (9.1) represents a conservative system with periodic motion for shearing, the free shearing motion starting from (K_0, K_0') is equivalent to its free motion from rest at either extreme shearing K_1 or K_2 so that $(K_0, K_0') = (K_1, 0) = (K_2, 0)$. By selecting $(K_1, 0)$ as our initial condition we find from (9.53) that $\xi_0 = \xi(K_1) = 0$, and the solution (9.58) reduces to

$$\hat{t} = \pm\frac{\tau^*}{2\pi}\sqrt{\frac{2}{\beta Q_1 Q_2}}F(\xi, k). \tag{9.60}$$

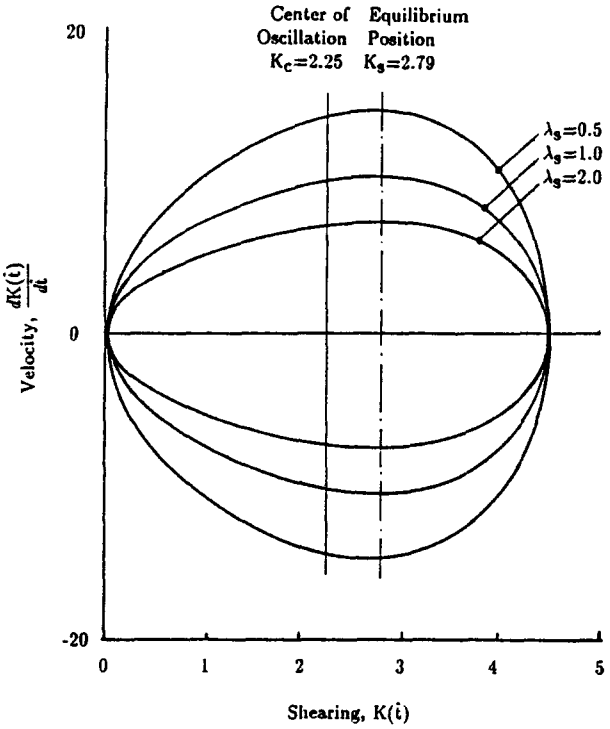

Fig. 9.14. Phase plane diagrams of the finite amplitude shearing motions of a quadratic oscillator on an inclined surface for $\beta = 0.5$, $K_1 = 0$, $K_2 = 4.5$, and for selected values of λ_s.

By introducing

$$\chi \equiv \frac{2\pi}{\tau^*}\sqrt{\frac{\beta Q_1 Q_2}{2}}, \tag{9.61}$$

we may write (9.60) in the form

$$\hat{t} = \pm\frac{1}{\chi}F(\xi, k) \tag{9.62}$$

so that

$$\xi = \pm \operatorname{sn} \chi\hat{t} = \pm \operatorname{sn}(\chi\hat{t}, k). \tag{9.63}$$

Hence, by (9.54) we finally find the solution to (9.1) for finite shearing:

$$K = \frac{K_1 Q_2 + K_2 Q_1 \tan^2(\frac{1}{2}\operatorname{sn}\chi\hat{t})}{Q_2 + Q_1 \tan^2(\frac{1}{2}\operatorname{sn}\chi\hat{t})}. \tag{9.64}$$

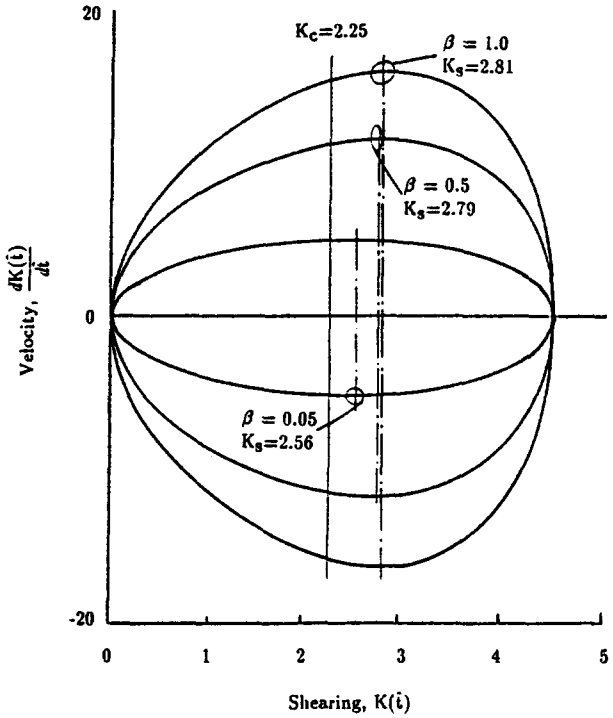

Fig. 9.15. Phase plane diagrams of the finite amplitude shearing motions of a quadratic oscillator on an inclined surface for $\lambda_s = 0.5$, $K_1 = 0$, $K_2 = 4.5$, and for selected values of β.

We see that K is a periodic function of the normalized time $\hat{t}$ with period of $(4/\chi)F(\pi/2, k)$.

We now consider the special case of $\beta = 0$ so that the motion becomes linear. It may be shown that

$$\beta Q_1 Q_2 = 2, \quad \chi = \frac{2\pi}{\tau^*} = \omega_K, \quad k = 0, \quad \xi = \cos^{-1}\left[\frac{(K_2 + K_1) - 2K}{K_2 - K_1}\right]. \tag{9.65}$$

Since $F(\xi, 0) = \xi$, we find from (9.62) $\xi = \pm\chi\hat{t}$. Hence, $(9.65)_4$ yields

$$K = \tfrac{1}{2}(K_2 + K_1) - \tfrac{1}{2}(K_2 - K_1)\cos\omega_K\hat{t}. \tag{9.66}$$

Solution (9.66), which can also be obtained from (9.64), shows that the finite shearing for a linear oscillator vibrates harmonically between two extreme positions K_1 and K_2 about its equilibrium position located in the middle of K_1 and K_2.

For the nonlinear spring we see its solution (9.62) is similar to (9.5) for oscillations on a smooth horizontal surface. The exact solutions of both cases

for the travel time $\hat{t}$ are found in terms of the elliptic integral of the first kind. The only difference between them is the equilibrium position. This difference is reflected from the different forms of the solution for K given by (9.64) and (9.8). If we let $\gamma = 0$ in (5.3) so that $\hat{g} = 0$ by $(7.14)_2$, it may be shown from (9.31), (9.39), (9.55), (9.57), and (9.61) that

$$K_s = 0, \quad K_1 + K_2 = 0, \quad Q_1 = Q_2 = \sqrt{2\left(K_1^2 + \frac{1}{\beta}\right)},$$
$$\chi = \omega_K \sqrt{1 + \beta K_1^2}, \quad k = K_1 \sqrt{\frac{\beta}{2(1 + \beta K_1^2)}}. \tag{9.67}$$

On the other hand, it is shown from (9.6) that

$$v = \omega_K \sqrt{1 + \beta K_0^2}, \quad \kappa = K_0 \sqrt{\frac{\beta}{2(1 + \beta K_0^2)}}. \tag{9.68}$$

By comparing $(9.67)_{4,5}$ and (9.68) we see that (9.62) reduces to (9.5) and (9.64) reduces to (9.8) since $K_0 = K_1$ is the initial condition in obtaining (9.62). Hence, the closed form solution (9.64) contains (9.8) as a special case.

Using (9.63) and (9.64) in (9.2) yields

$$H'' + A(\xi)H = 0, \tag{9.69}$$

where the periodic function $A(\xi)$ is given by

$$A(\xi) = \omega_H^2 + \mu_H \left[\frac{K_1 Q_2 + K_2 Q_1 \tan^2\left(\frac{\xi}{2}\right)}{Q_2 + Q_1 \tan^2\left(\frac{\xi}{2}\right)} \right]^2 \tag{9.70}$$

We shall again follow the approach used in the previous chapters to study the stability property of small torsional motion governed by (9.69). In view of (9.58) and (9.61), we introduce the transformation

$$\hat{t} = \frac{1}{\chi} \left[\int_0^{\xi} \frac{d\phi}{\sqrt{1 - k^2 \sin^2 \phi}} - \int_0^{\xi_0} \frac{d\phi}{\sqrt{1 - k^2 \sin^2 \phi}} \right] \tag{9.71}$$

to reduce equation (9.69) to

$$\frac{d^2 H}{d\xi^2} + 2P(\xi) \frac{dH}{d\xi} + R(\xi) H = 0, \tag{9.72}$$

where

$$P(\xi) = -\frac{1}{2}\frac{k^2 \sin\xi \cos\xi}{1 - k^2 \sin^2\xi}, \tag{9.73}$$

$$R(\xi) = \frac{d^2}{\beta Q_1 Q_2 \lambda_s (1 - k^2 \sin^2\xi)} \times \left[1 + 2\beta\left[\frac{(K_1 Q_2 + K_2 Q_1) + (K_1 Q_2 - K_2 Q_1)\cos\xi}{(Q_2 + Q_1) + (Q_2 - Q_1)\cos\xi}\right]^2\right]. \tag{9.74}$$

In deriving (9.74), we used the definitions of ω_K, ω_H, μ_H, and χ defined through (7.12–14), $(9.37)_2$, and (9.61). Now using substitution

$$H = y \exp\left(-\int^{\xi} P(\phi)\, \mathrm{d}\omega\right) \tag{9.75}$$

in (9.72), we obtain the equation of motion in the form

$$\frac{\mathrm{d}^2 y}{\mathrm{d}\xi^2} + D(\xi) y = 0, \tag{9.76}$$

where

$$D(\xi) = R(\xi) - P^2(\xi) - \frac{\mathrm{d}P(\xi)}{\mathrm{d}\xi}. \tag{9.77}$$

Using (9.73) in (9.75) yields

$$H = \frac{y}{(1 - k^2 \sin^2\xi)^{1/4}}, \tag{9.78}$$

which is the specific form of the transformation we used in reducing (9.72) to (9.76). This very same transformation has been used twice in the previous sections in (8.45) and (9.25). Using (9.73), and (9.74) in (9.77), we find

$$D(\xi) = \frac{d^2}{\beta Q_1 Q_2 \lambda_s (1 - k^2 \sin^2\xi)} \times \left[1 + 2\beta\left[\frac{(K_1 Q_2 + K_2 Q_1) + (K_2 Q_2 - K_2 Q_1)\cos\xi}{(Q_2 + Q_1) + (Q_2 - Q_1)\cos\xi}\right]^2\right] - \frac{k^2(1 + \sin^2\xi)}{4(1 - k^2 \sin^2\xi)} + \frac{3k^2 \cos^2\xi}{4(1 - k^2 \sin^2\xi)^2}. \tag{9.79}$$

Hence, $D(\xi)$ is an even function of period 2π. From (9.53) we see that when K oscillates between its two extreme positions K_1 and K_2, ξ moves between 0 and π. Hence, we only need to consider the function $D(\xi)$ for $\xi \in [0, \pi]$. The difference between (9.76) and (9.23) is the forms of the function D, which is shown by (9.79) and (9.26) respectively. In this case, bearing in mind the previous relations, $D(\xi)$ depends on the following parameter:

$$k^2 = \frac{(K_1 - K_2)^2 - (Q_1 - Q_2)^2}{4Q_1 Q_2}. \tag{9.80}$$

By (9.55) we see that this parameter and $D(\xi)$ as a function of ξ in turn depend on β, λ_s, d, K_1, and K_2. Here we again follow Beatty and Bhattacharyya's approach [4] outlined in §8.2 to conduct the stability analysis through numerical calculation. For all of our numerical calculations, we assume $K_1 = 0$ for the convenience of illustration. In other words, we assume that one of the extreme shear deflections was located at the unsheared position. Using the stability criterion developed by Bhattacharyya [10], we conducted numerical calculations for a wide range of parameters

$$\lambda_s \in [0.2, 2], \quad \beta \in [0.05, 1], \quad d \in [0.01, 10], \quad K_2 \in [0.01, 10]. \tag{9.81}$$

It is found again that the Fourier coefficients for $D(\xi)$ converge very fast. Actually, the first two terms approximate $D(\xi)$ very well. This indeed shows again that the dynamical behavior of small torsional motion coupled with finite shearing is very close to that of Mathieu's equation.

The stability maps for small torsion coupled with finite shearing are provided in Figs. 9.16–9.19 with the shaded areas representing the unstable regions in the $d - K_2$ space. It is shown that the unstable regions resemble the ones in §8.2.1. As λ_s increases, the unstable regions shift in the positive d direction. When β increases as the nonlinearity of the material becomes stronger, the unstable region becomes larger, as shown in the figures.

Figure 9.20 is the result of numerical integration of equations (9.1) and (9.2). The constant gravitational force is replaced by two extreme shear deflections K_1 and K_2 through (9.39). The physical parameters used in this calculation are $\beta = 0.5$, $\lambda_s = 1$, $d = 1.5$, $K_s = 1$, $K_1 = 0$, $K_2 = 5.0$, and with initial data of $(K_0, K_0') = (5, 0)$ and $(H_0, H_0') = (0.5, 0)$. This point falls into the unstable region on the stability map in Fig. 9.17. We see that the small torsional motion builds up and approaches infinity. The corresponding exact numerical solution of equations (7.9) and (7.10) shows, however, coupled motion similar to that in Fig. 8.15.

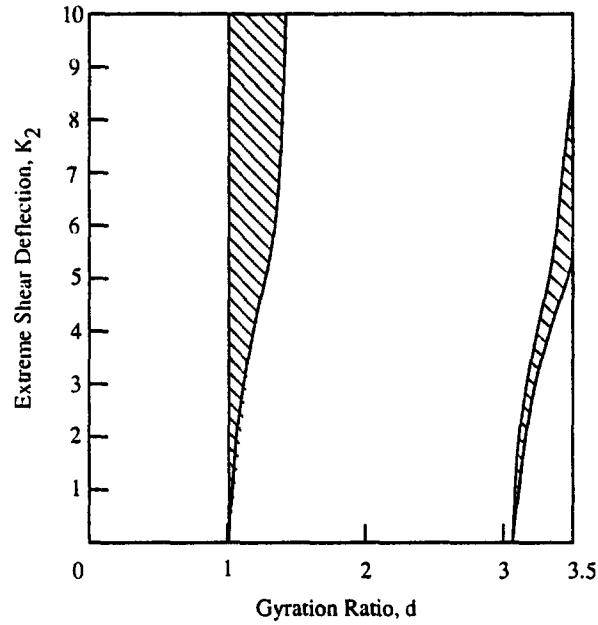

Fig. 9.16. Stability map of small torsional motion on an inclined surface coupled with finite amplitude shearing vibrations of a quadratic oscillator for $K_1 = 0$, $\beta = 0.5$, and $\lambda_s = 0.5$. The shaded areas are the unstable regions.

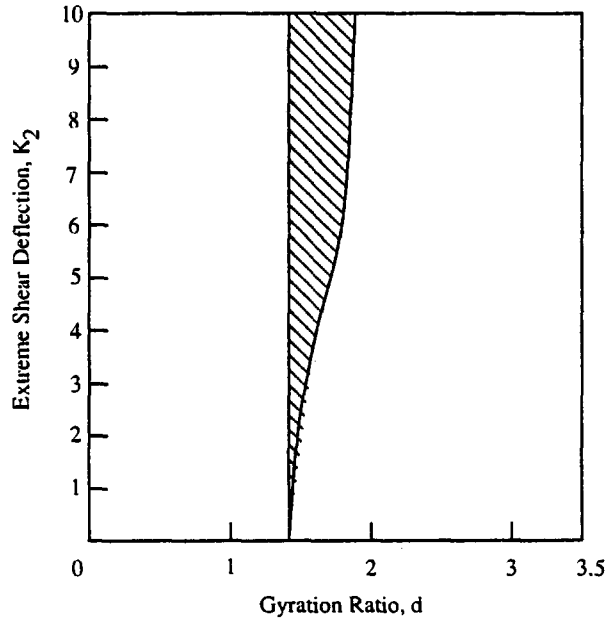

Fig. 9.17. Stability map of small torsional motion on an inclined surface coupled with finite amplitude shearing vibrations of a quadratic oscillator for $K_1 = 0$, $\beta = 0.5$, and $\lambda_s = 1.0$. The shaded areas are the unstable regions.

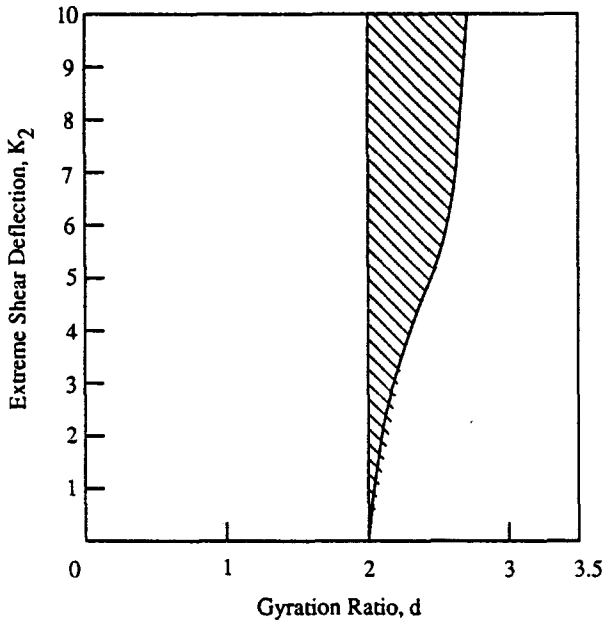

Fig. 9.18. Stability map of small torsional motion on an inclined surface coupled with finite amplitude shearing vibrations of a quadratic oscillator for $K_1 = 0$, $\beta = 0.5$, and $\lambda_s = 2.0$. The shaded areas are the unstable regions.

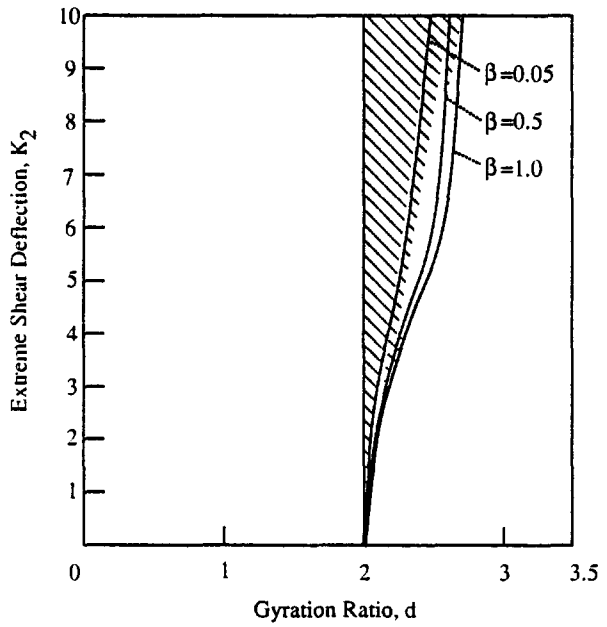

Fig. 9.19. Stability map of small torsional motion on an inclined surface coupled with finite amplitude shearing vibrations of a quadratic oscillator for $K_1 = 0$, $\lambda_s = 2.0$, and selected values of β. The shaded areas are the unstable regions.

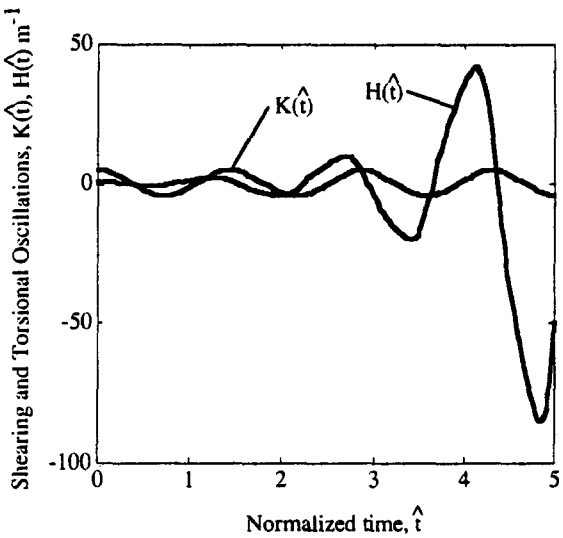

Fig. 9.20. Finite shearing and small torsional motions of a quadratic oscillator on an inclined surface with $\beta = 0.5$, $\lambda_s = 1$, $d = 1.5$, $K_1 = 0$, $K_2 = 5$, and $K_s = 1$. This point falls into the unstable region on the stability map in Fig. 9.17.

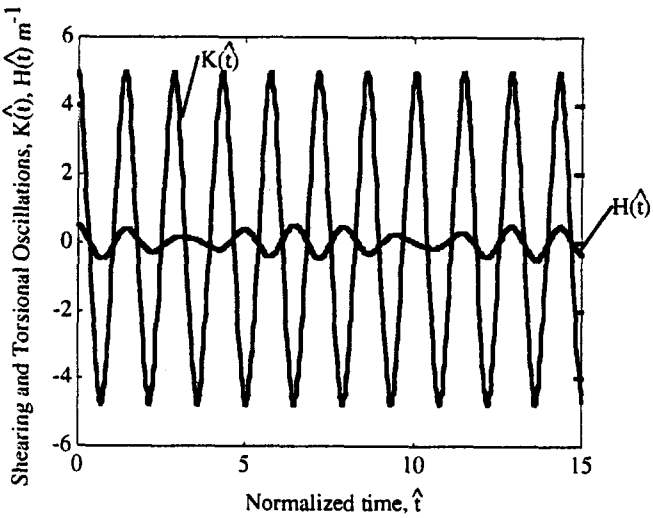

Fig. 9.21. Finite shearing and small torsional motions of a quadratic oscillator on an inclined surface with $\beta = 0.5$, $\lambda_s = 1$, $d = 1$, $K_1 = 0$, $K_2 = 1$, and $K_s = 1$. This point falls into the stable region on the stability map in Fig. 9.7. The initial data: $(K_0, K_0') = (5, 0)$, $(H_0, H_0') = (0.5, 0)$.

Figure 9.21 shows another numerical integration of equations (9.1) and (9.2) for $\beta = 0.5$, $\lambda_s = 1.0$, $d = 1.0$, $K_s = 1$, $K_1 = 0$, $K_2 = 1.0$ and for the initial data of $(K_0, K_0') = (5, 0)$ and $(H_0, H_0') = (0.5, 0)$. This point falls into the stable region. The oscillations for both torsion and shearing are periodic and independent of each other.

Acknowledgement

This work was supported first by a grant from the National Science Foundation awarded to Potomac State College and then by a West Virginia EPSCoR grant from the National Science Foundation while the author was a faculty member at the Potomac State College of West Virginia University.

References

1. C. Truesdell and W. Noll, *The Nonlinear Field Theories of Mechanics*. Flügge's Handbuch der Physik III/3, Berlin, Heidelberg, New York: Springer-Verlag (1965).
2. M.F. Beatty, Finite amplitude, periodic motion of a body supported by arbitrary isotropic, elastic shear mountings. *J. Elasticity* 20 (1988) 203–230.
3. M.F. Beatty, Stability of a body supported by a simple vehicular shear suspension system. *Int. J. Non-Linear Mechanics* 24/1 (1989) 65–77.
4. M.F. Beatty and R. Bhattacharyya, Poynting oscillations of a rigid disk supported by a neo-Hookean rubber shaft. *J. Elasticity* 24 (1990) 135–186.
5. M.F. Beatty, Topics in finite elasticity: Hyperelasticity of rubber, elastomers, and biological tissues – with examples. *Applied Mech. Revs.* 40 (1987) 1699–1734.
6. M.F. Beatty, Finite amplitude vibrations of a body supported by simple shear springs. *ASME J. Appl. Mech.* 51 (1984) 361–366.
7. M.F. Beatty, A class of universal relations in isotropic elasticity theory. *J. Elasticity* 17 (1987) 113–121.
8. J.J. Stoker, *Nonlinear Vibrations in Mechanical and Electrical Systems*. New York: Interscience Publishers, Inc. (1950).
9. E.T. Whittaker and G.N. Watson, *A Course of Modern Analysis*. Cambridge University Press, Cambridge (1952).
10. R. Bhattacharyya, A stability criterion for the Mathieu-Hill equation, University of Kentucky Tech. Rpt. (Jan. 1988).
11. M.F. Beatty and A.C. Chow, Finite amplitude vibrations of a Mooney-Rivlin oscillator. *Arch. Rational Mech. Anal.* 102/2 (1988) 141–166.